PB2001-106552

Testing of Multifrequency Radar Algorithm for the Detection of Aircraft Icing Potential With Aircraft-Sampled Cloud and Precipitation Data

May 2001

DOT/FAA/AR-TN01/3

U.S. Department of Transportation

Federal Aviation Administration

NOTICE

This document is disseminated under the sponsorship of the U.S. Department of Transportation in the interest of information exchange. The United States Government assumes no liability for the contents or use thereof. The United States Government does not endorse products or manufacturers. Trade or manufacturer's names appear herein solely because they are considered essential to the objective of this report. This document does not constitute FAA certification policy. Consult your local FAA aircraft certification office as to its use.

This report is available at the Federal Aviation Administration William J. Hughes Technical Center's Full-Text Technical Reports page: actlibrary.tc.faa.gov in Adobe Acrobat portable document format (PDF).

Technical Report Documentation Page

1. Report No.	2. Government Accession No.	3. Recipient's Catalog No.
DOT/FAA/AR-TN01/3		

4. Title and Subtitle	5. Report Date
TESTING OF MULTIFREQUENCY RADAR ALGORITHM FOR THE DETECTION OF AIRCRAFT ICING POTENTIAL WITH AIRCRAFT-SAMPLED CLOUD AND PRECIPITATION DATA	May 2001
	6. Performing Organization Code
7. Author(s)	8. Performing Organization Report No.
Dr. Andrew L. Pazmany and Dr. James B. Mead	
9. Performing Organization Name and Address	10. Work Unit No. (TRAIS)
Quadrant Engineering Inc. 107 Sunderland Road Amherst, MA 01002	11. Contract or Grant No.
12. Sponsoring Agency Name and Address	13. Type of Report and Period Covered
U.S. Department of Transportation Federal Aviation Administration Office of Aviation Research Washington, DC 20591	Technical Note
	14. Sponsoring Agency Code AIR-100

15. Supplementary Notes

The Federal Aviation Administration William J. Hughes Technical Center COTR was Edward Pugacz.

16. Abstract

In 1997, Quadrant Engineering Inc. (QEI) proposed a neural network algorithm for the estimation of cloud and precipitation parameters such as Liquid Water Content (LWC) and drop size from multifrequency radar measurements. QEI was subsequently commissioned to evaluate the performance of the technique with real, aircraft-sampled cloud and precipitation drop size distributions. QEI simulated the radar signals at various frequencies using the aircraft-sampled drop size distributions, processed the radar signals with an artificial neural network, and compared the neural net estimated cloud and precipitation parameters with the actual parameters measured by the aircraft. Ice particles present in some of the sampled clouds and precipitation were not included in the analysis. Results indicate that a combination of 10-95 or 10-35-95 GHz radars can measure LWC with 1-km range resolution with a standard error of less than 0.05 g/m^3 and drop size to within 50% error in high signal-to-noise-ratio conditions. The estimates of the 10-35 GHz radar combination were not as accurate in similar conditions but are expected to be effective in long range, coarse resolution (≥2 km) measurements.

17. Key Words	18. Distribution Statement
Multifrequency Radar, Aircraft icing potential, Liquid water content, Drop size, Neural network	This document is available to the public through the National Technical Information Service (NTIS), Springfield, Virginia 22161.

19. Security Classif. (of this report)	20. Security Classif. (of this page)	21. No. of Pages	22. Price
Unclassified	Unclassified	42	

TABLE OF CONTENTS

LIST OF FIGURES

LIST OF TABLES

DEFINITION OF VARIABLES

α	Shape parameter for gamma distribution; larger values of α yield a narrower distribution
c	Speed of light (2.997e8 m/s)
C	Correlation factor (0$<C<$1) to determine overlap between range gates
D	Particle diameter (m)
dBZ	Radar Reflectivity Factor; proportional to D^6
$dBZe$	Radar Equivalent Reflectivity Factor; radar measured dBZ assuming Rayleigh scatterers (used with millimeter wave radars when particles are often Mie scattered).
E_{LWC}	RMS error of the neural net estimated liquid water content (g/m^3)
E_{MVD}	Relative RMS error of the neural net estimated MVD (%)
E_{MZD}	Relative RMS error of the neural net estimated MZD (%)
f	Frequency (Hertz)
γ	Shape parameter for gamma distribution. Larger γ values yield narrower distributions
k_w	Extinction due to liquid water (dB/km)
K	Complex quantity related to the index of refraction of water or ice
λ	Electromagnetic wavelength (m)
L_a	Atmospheric loss (dB/km)
LWC	Liquid water content (g/m^3)
MD	Mean Diameter (μm)
MVD	Mean Volume Diameter (μm)
MZD	Mean Z Diameter (μm)
LWC_{NN}	Neural Net Estimated Liquid Water Content (g/m^3)
MVD_{NN}	Neural Net Estimated Mean Volume Diameter (μm)

MZD_{NN}	Neural Net Estimated Mean Z Diameter (μm)
η	Volume backscattering coefficient (m^2/m^3)
N	Index of refraction
N_i	Number of input nodes in neural network
N_r	Number of range gates sampled by neural network
N_f	Number of frequencies sampled by neural network
N_p	Number of output parameters of the neural network
N_o	Number of output nodes in neural network
N_{ave}	Number of radar samples averaged (power average)
N_0	Number density parameter for the Marshall-Palmer distribution
ϕ	General angular variable
ϕ_{az}	Scan range in azimuth (radians)
ϕ_{el}	Scan range in elevation (radians)
p(r)	Drop size distribution (number of drops per cubic meter per meter diameter)
P_t	Radar transmit power (W)
P_{rmin}	Minimum detectable received power (W)
r_c	Mode radius (radius corresponding to the peak value of the drop size distribution)
r	Particle radius (μm)
R	Radar range (m)
τ	Pulse length (s)
Z	Cloud reflectivity (mm^6/m^3). Z_{vv} is the copolarized reflectivity for transmission and reception of vertical polarization; Z_{hh} is the copolarized reflectivity for transmission and reception of horizontal polarization; and Z_{vh} is the cross-polarized reflectivity, for transmission of horizontal and reception of vertical polarization.

EXECUTIVE SUMMARY

This report addresses the results obtained in the application of a neural network algorithm employing simulated radar signals to ascertain the icing potential of various cloud/participation parameters. In 1997, a study was conducted to assess remote sensing techniques for the detection and mapping of aircraft icing potential. After analyzing a variety of active and passive remote sensor combinations, multifrequency radar was identified as the most promising technology to address the problem. The technique involves simultaneous processing of 10, 35, and 95 GHz radar reflectivity profiles with an artificial neural network to estimate liquid water content (LWC) and drop size in clouds and precipitation. Computer simulations indicated that LWC, mean volume diameter (MVD), and mean z diameter (MZD) can be estimated with reasonable accuracy, even in the presence of significant (1 dB) measurement errors. To further investigate this technique, the Federal Aviation Administration (FAA) in collaboration with the National Aeronautics and Space Administration Glenn Research Center (NASAGRC) and the U.S. Army Corps of Engineers Cold Regions Research and Engineering Laboratory (CRREL), commissioned Quadrant Engineering Inc. (QEI) to test the neural network algorithm with real cloud and precipitation data. QEI was provided aircraft-sampled drop size distributions, which were processed into profiles of actual LWC, MVD, MZD, and corresponding profiles of radar reflectivity at each radar frequency. The radar reflectivity profiles were then processed with the neural network to estimate LWC, MVD and, MZD. It was found that the three-frequency neural network estimated LWC to within 0.1 g/m^3 (for a data set with a mean LWC 0.152 g/m^3), MVD to within 90%, and MZD to within 40% compared to the parameters measured by the aircraft probes. The tests also revealed that a 10-95 GHz radar performance in liquid clouds and precipitation is similar to that of a three-frequency system.

The multifrequency technique is not as well suited to measure the size parameter MVD as MZD, which is more strongly affected by the largest drops that dominate reflectivity. Neither of these parameters are necessarily correlated with the more conventional MVD, particularly for bimodal drop size distributions. The MVD behaved very erratically for the bimodal distributions analyzed.

The results also indicate that in small (Rayleigh) drop size and high LWC conditions, the 10-35-95 or 10-95 GHz radar combinations can effectively estimate LWC, MVD, and MZD at finer than 1-km range resolution. The potential benefit of this capability is that in the most hazardous conditions, an operational system will be able to provide pilots and ground crew more resolved maps of the spatial extent and intensity of icing potential.

Median volume diameter, denoted by MeVD in this report, is the droplet size parameter used in icing certification, icing wind tunnels, and ice accretion codes. It was investigated as part of the study, but no results are included in the report. The parameter was found to behave erratically for bimodal distributions, which were reasonably well represented in the data set and are believed to be not uncommon in supercooled large droplet (SLD) conditions in the atmosphere.

It is expected that the accuracy of the estimated liquid cloud and precipitation parameters will depend on:

1. Matching the sample volumes of the different radar frequencies.

2. The precision of radar reflectivity measurements (a function of signal-to-noise ratio, the number of independent samples averaged, and nonlinearity of the radar receiver).

3. Variations in Mie scattering (due to large particles) from range cell to range cell.

4. Absolute calibration of the X-band channel.

5. Ice water content in the radar sample volume.

For this study, ice particles present in the real cloud and precipitation rate were not included in the analysis.

Work is now under way to test the multifrequency radar technique with real radar measurements. During the Mount Washington Icing Sensors Project, April 1999 (MWISP '99), coincident 10-, 35-, and 95-GHz radar reflectivity profiles and corresponding in situ observations were collected in conditions ranging from drizzle to mixed phase and ice clouds. Also, the Alliance Icing Research Study (AIRS 1999) was conducted in Mirabel, Quebec, where weather conditions were favorable for the observation of supercooled liquid clouds and drizzle.

BACKGROUND

STATEMENT OF THE PROBLEM.

In 1997, a study was conducted to assess remote sensing techniques for the detection and mapping of aircraft icing potential [1]. The problem was constrained to a forward-looking volume imaging remote sensing system capable of measuring cloud and precipitation parameters such as liquid water content (LWC) and drop size at about 1-km range resolution out to 20-30 km. The measurement concept for an in-flight sensor system is illustrated in figure 1.

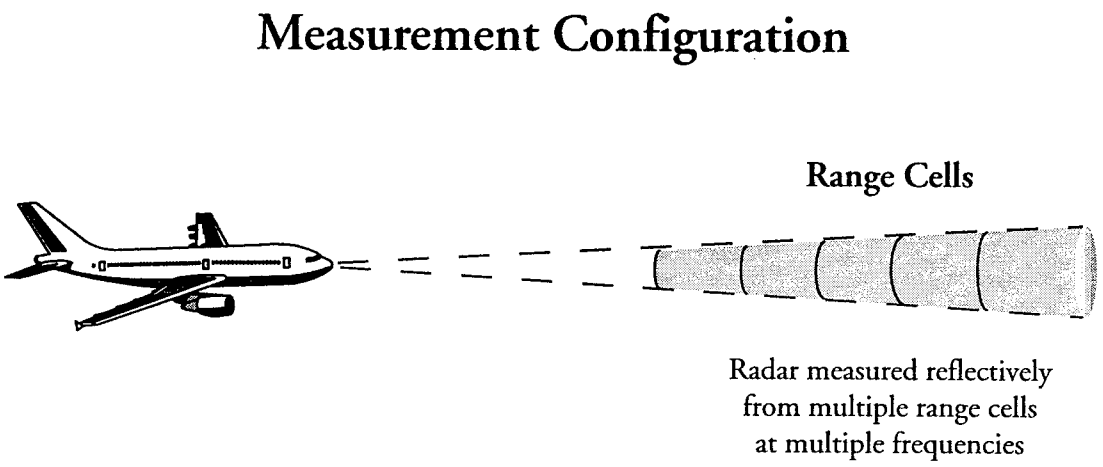

FIGURE 1. MEASUREMENT CONCEPT OF AN IN-FLIGHT ICING DETECTION REMOTE SENSING SYSTEM

After analyzing a variety of active and passive remote sensor combinations, multifrequency radar was identified as the most promising technology for the problem. The technique involves the simultaneous processing of 10, 35, and 95 GHz radar reflectivity profiles with an artificial neural network to estimate LWC and drop size in clouds and precipitation. Computer simulations indicated that LWC, drop size (measured as medium volume diameter (MVD)), and mean z diameter (MZD) can be estimated with reasonable accuracy, even in the presence of significant (1 dB) estimation errors. The procedure of this computer simulation is summarized in figure 2. The simulation first generated a large set of artificial cloud and precipitation conditions, specified in terms of profiles of drop size distributions. From these drop size distributions, the computer algorithm then calculated the corresponding radar observed reflectivity profiles at each operating frequency as well as LWC and drop size in each volume cell. This set of multifrequency radar reflectivity (inputs) and cloud and precipitation parameter profiles (outputs) were then used to train an artificial neural network. A statistically independent, but still simulated, data set was used to evaluate the ability of the neural net to estimate LWC and drop size from the radar data.

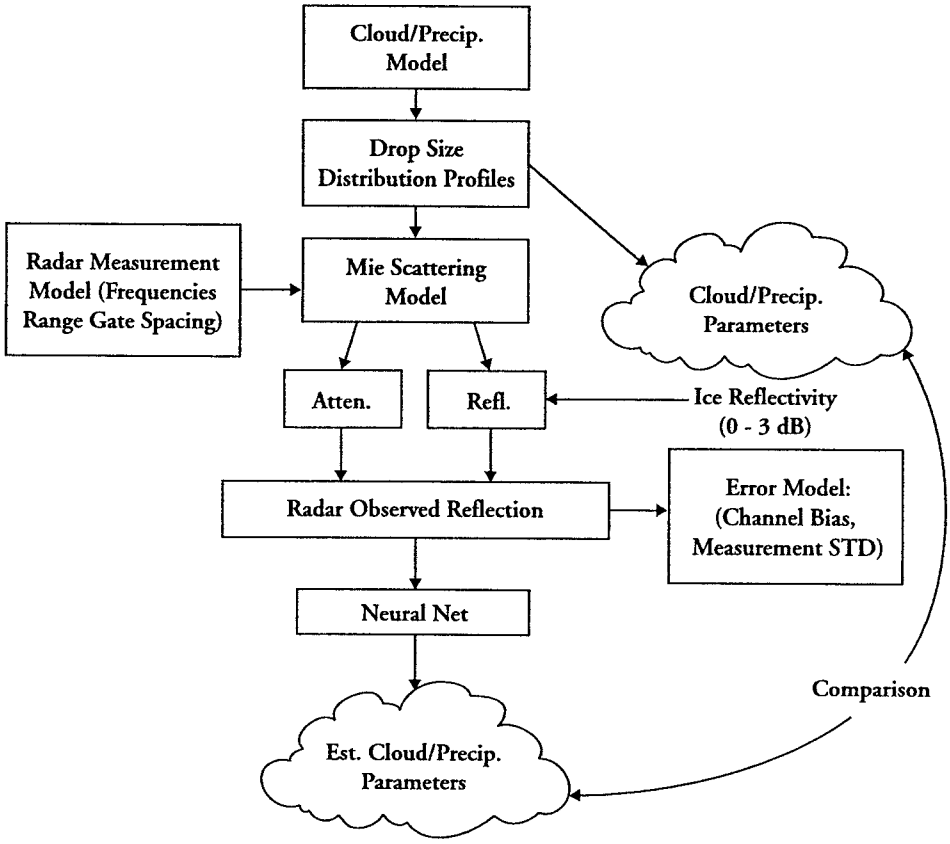

FIGURE 2. EVALUATION OF THE MULTIFREQUENCY RADAR TECHNIQUE FOR THE MEASUREMENT OF CLOUD AND PRECIPITATION PARAMETERS WITH SIMULATED DATA

MULTIFREQUENCY RADAR.

Multifrequency radar has an excellent potential for probing cloud particle parameters due to the combination of moderate attenuation and adequate scattering cross section. In the original 1998 study, Quadrant Engineering Inc. (QEI) formulated a working hypothesis that cloud parameters could be extracted by measuring backscatter at a combination of attenuating and nonattenuating frequencies. Since scattering is a complex nonlinear function of particle size and frequency, it is impractical to consider an analytical solution to the inverse problem of computing particle size and liquid water content based on measured backscattered power at multiple frequencies. QEI, therefore, focused its efforts on an approximate numerical solution to the inversion, specifically, a neural network. The network was trained by simulating thousands of test cases of radar scattering from assumed particle size distributions.

The inverse problem of extracting cloud parameters from the measured range profiles of backscattered power is a good example of a problem without well defined rules for estimation. The forward problem is straightforward—for a given drop size distribution, reflectivity and attenuation can easily be calculated using Mie scattering formulas. Also, cloud and precipitation properties, such as LWC or rain rate, can be directly calculated from drop size distribution.

Solving the inverse problem, that is, calculating cloud parameters from measured reflectivity profiles, is very difficult, due to the nonlinearity of the forward problem. Neural nets are ideal for solving problems where the forward problem is well characterized but the inverse is nonlinear and complicated.

PROCEDURE

TEST DATA SET.

The objective of this study was to further test the multifrequency radar technique with real cloud and precipitation data. The original QEI study [1] was conducted with simulated cloud and precipitation data based on the Gamma drop size distribution model [2], which does not include irregular, multimodal distribution shapes. Real conditions of course do include such shapes. Moreover, it was assumed that the weather conditions were somewhat correlated from range cell to range cell. It is uncertain how well this model represents real world conditions and therefore, the validity of the results of the original study came into question. To test the algorithm with real cloud and precipitation data, the Federal Aviation Administration (FAA) in collaboration with the National Aeronautics and Space Administration Glenn Research Center (NASAGRC) and the U.S. Army Corps of Engineers Cold Regions Research and Engineering Laboratory (CRREL), provided QEI with 244 aircraft-sampled drop size distributions. Each distribution corresponds to a segment of data collected during a flight leg. The time interval between segments is anywhere from a few seconds to several days. The data set was collected during the Supercooled Large Droplet (SLD) Icing Research Flights, on January 24 and 27 and March 20, 1997 and February 4, 1998, as part of the FAA/NASA/National Center for Atmospheric Research (NCAR) SLD Icing Flight Research Program, in conditions ranging from clouds to drizzle and rain. The 244 drop size distributions were processed into five range gate profiles of actual LWC, MVD, MZD, and corresponding profiles of radar reflectivity at each radar frequency. The radar reflectivity profiles were then processed with the neural network to estimate LWC, MVD, and MZD. Ice particles were present in some of the sampled clouds and precipitation, but were not included in the analysis.

No results are presented in this report for median volume diameter (MeVD). In light of its prominent role in aircraft icing engineering, it was investigated. However, it was found that a fair percentage of the drop size distributions were bimodal and that the MeVD behaved erratically for these distributions, in one case jumping between 20 and 400 microns for just about identical cloud/drizzle conditions. MeVD tends to approximate MVD for unimodal distributions, but not for bimodal distributions. Thus, results presented in this report for MVD cannot be taken as representative of MeVD. The definition of MeVD suggests that it may be incompatible with the integrated measurements of remote sensors, and this investigation lends support to that view.

The scatter plots of LWC vs MVD and MVD vs mean diameter (MD) seen in figures 3 and 4 illustrate the distribution of the data. The data set was subdivided into three regions to examine algorithm performance in specific conditions: (1) small drops, low LWC (MVD < 300 micrometers, LWC < 0.2 g/m^3); (2) large drops (MVD > 300 micrometers); and (3) small drops,

large LWC (MVD < 300 micrometers, LWC > 0.2 g/m^3). The thresholds were chosen to correspond to apparent natural breaks in the data.

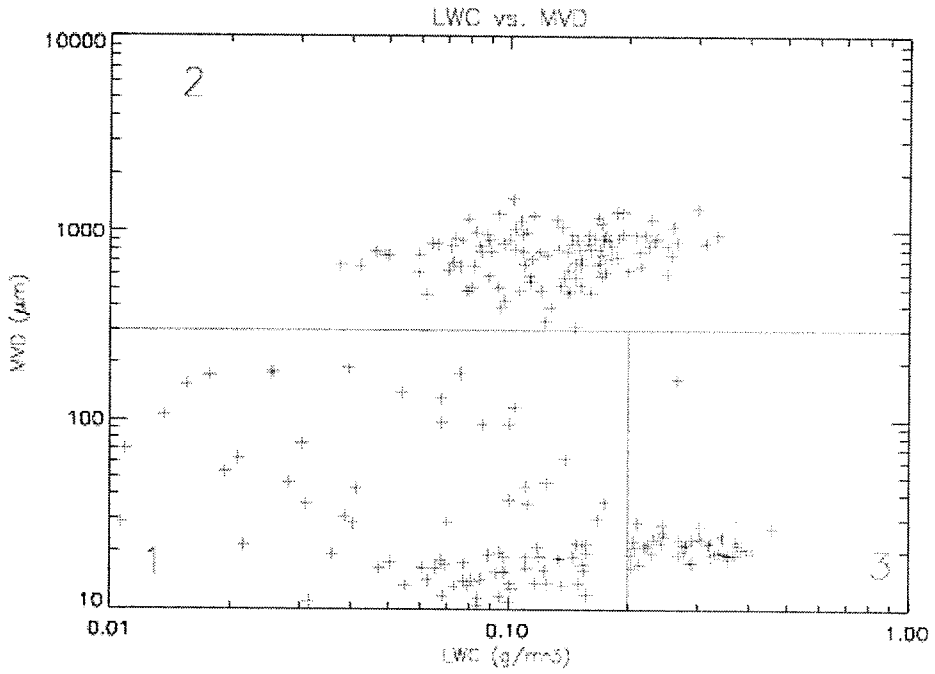

FIGURE 3. LIQUID WATER CONTENT (LWC) VS MEAN VOLUME DIAMETER (MVD) SCATTER PLOT OF THE TEST DATA SET (Aircraft-sampled drop size distributions)

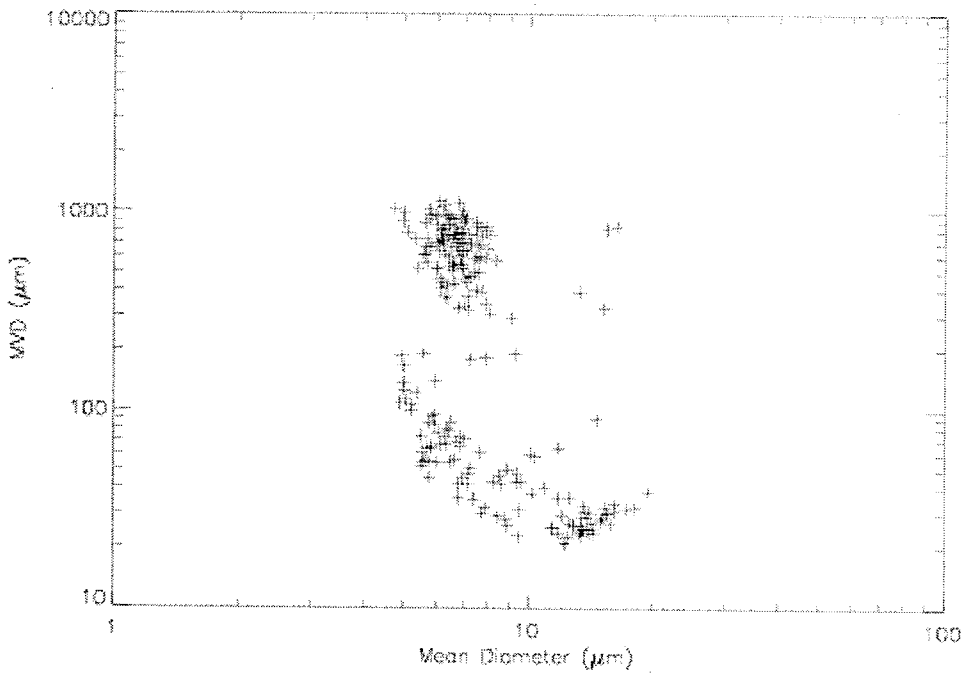

FIGURE 4. MEAN DIAMETER (MD) VS MVD SCATTER PLOT OF TEST DATA (Wide distributions are indicated by a significant difference between MVD and MD.)

Many points in figure 4 indicate a great difference between MVD and MD, which suggests a large number of wide size distributions. Closer examination of individual distributions revealed that many of these wide distributions had bimodal shapes. One of these is plotted in figure 5.

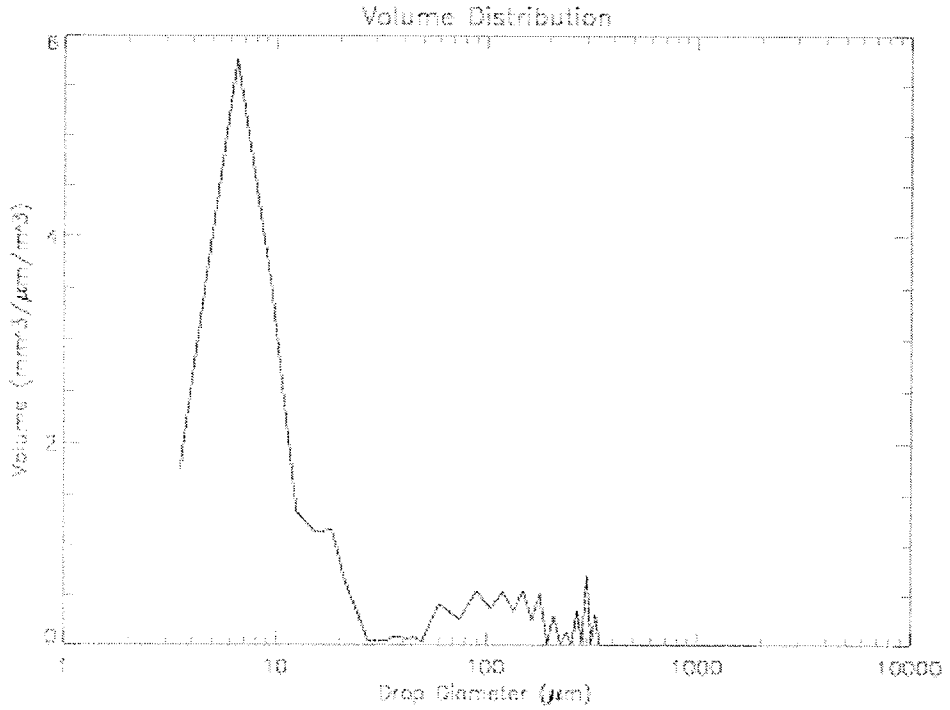

FIGURE 5. A BIMODAL DROP SIZE DISTRIBUTION OF THE NASA TEST DATA SET

The 244 drop size distributions were grouped into 240, five element profiles. First, the 244 distributions were arranged according to increasing time; the distribution with the earliest time stamp was the 1st and the one with the last was the 244th. Then the first profile was constructed using the 1st, 2nd ... 5th drop size distributions, the second profile using the 2nd, 3rd ... 6th distribution, and so on until the last, 240th profile was formed with the 240th, 241st ... 244th distribution. This was done to try to reconstruct the spatial variability in the cloud and precipitation conditions along the aircraft flight line. Since the data was collected over long flight segments, the majority of distribution sequences well represent this spatial variation, on scales similar to the range resolution used in the simulations. The procedure for the analysis was similar to the original computer simulation but with real drop size distribution. This procedure is illustrated in figure 6.

Using Mie scattering and extinction equations, the radar-observed reflectivity profiles were calculated (including attenuation), as well as corresponding "actual" LWC, MVD, and MZD for each range cell (range gate). The calculated radar reflectivity profiles were then entered as inputs to the neural network to estimate cloud parameters. The neural net, again, estimated the cloud parameters in the middle three range cells (in the 2nd, 3rd, and 4th range gates).

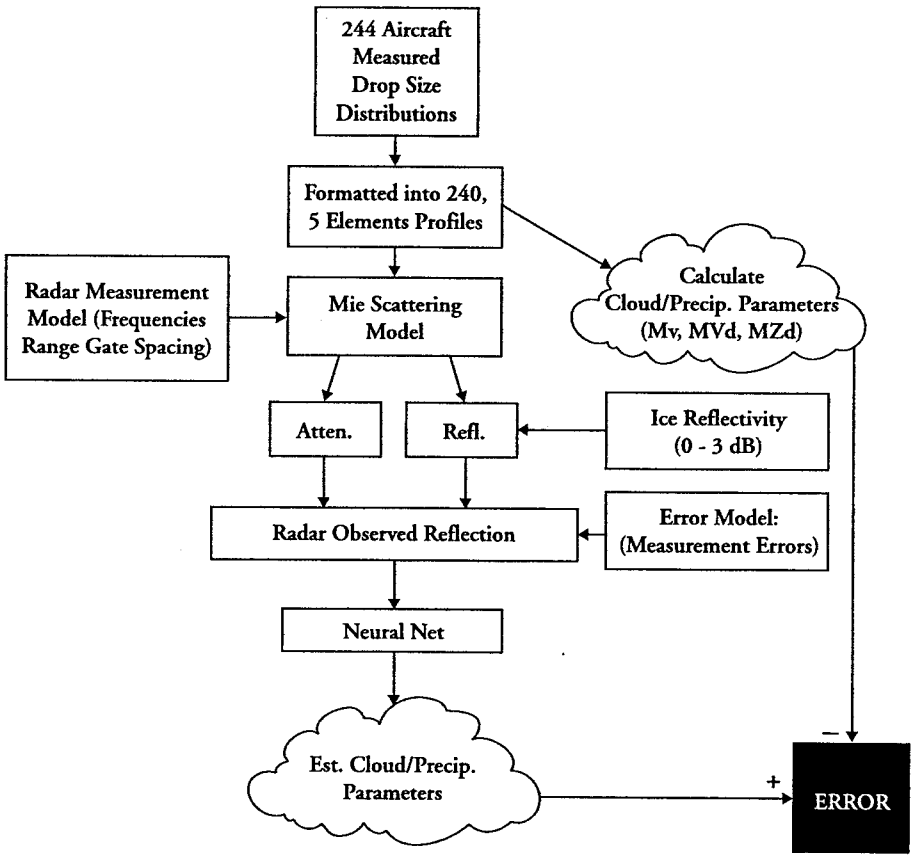

FIGURE 6. PROCEDURE FOR THE EVALUATION OF THE MULTIFREQUENCY TECHNIQUE WITH REAL CLOUD AND PRECIPITATION DATA

NEURAL NETWORK AND THE SYNTHETIC TRAINING DATA SET.

The neural network topography used in this study was the same as in the original study [1] carried out by QEI. The three-frequency network consisted of 15 input nodes (five range gates at three frequencies), a 20- and a 12-node hidden layer, and a 9-node output layer. The two-frequency networks had 10 input nodes, a 15- and a 12-node hidden layer and, again, a 9-node output layer. The nine outputs were LWC, MVD and MZD, corresponding to the middle three (out of five) range gates. The net topology, training, and data processing were implemented with the Stuttgart Neural Network Simulator (SNNS) [3] software executed on a PC computer running the Linux 6.0 operating system.

In the original study, the multifrequency reflectivity profiles were directly used as inputs to the neural net. This type of configuration, however, must assume absolutely calibrated and unattenuated reflectivity measurements in the first range gate at all frequencies. This is an unnecessary constraint on the algorithm and an unrealistic requirement on the easily attenuated millimeter wavelength reflectivity measurements. The primary need for millimeter wave data is to estimate LWC from differential reflectivity gradients that can be derived from uncalibrated radar profiles. The neural network input data was, therefore, slightly modified in this study. The five-element (5 range gates) radar equivalent reflectivity factor vectors, Z_{Ka} and Z_W, in units of

dBZe, were combined to calculate the following two, five-element differential reflectivity gradient vectors, ΔZ_{X-Ka} and ΔZ_{X-W}, normalized to the first element:

$$\Delta Z_{X-Ka} = Z_X - Z_{Ka} - [Z_X(1) - Z_{Ka}(1)] \text{ (dB)}$$

and

$$\Delta Z_{X-W} = Z_X - Z_W - [Z_X(1) - Z_W(1)] \text{ (dB)}$$

where Z_X (1), Z_{Ka} (1), and Z_W (1) represent radar observed reflectivity factors in the first range gate of the X, Ka, and W-band radars in *dBZe*. Note that the three-frequency net was applied to all three vectors, Z_X, ΔZ_{X-Ka}, and ΔZ_{X-W}, while the two-frequency 10-35 GHz and 10-95 GHz nets only used vectors $[Z_X, \Delta Z_{X-Ka}]$ and $[Z_X, \Delta Z_{X-W}]$.

The neural networks were trained with the simulated liquid cloud and precipitation model based on modified gamma drop size distribution [2] but tested with radar reflectivity and cloud parameters generated from real drop size distributions. The modified gamma distribution relates liquid drop diameters to the number of drops per drop size interval in a unit volume according to:

$$f(D) = a\left(\frac{D}{2}\right)^{\alpha} e^{-b\left(\frac{D}{2}\right)^{\gamma}}$$

where

$f(D)$ is the drop size distribution in units of the number of drops per micron per m^3

$$a = \frac{3LWC\gamma b^{b_2}}{4e^6\pi\Gamma(b_2)}$$

$$b = \frac{\alpha}{\gamma R_c^{\gamma}}$$

$$b_2 = \frac{\alpha + 4}{\gamma}$$

and α and γ are shape parameters, D is the drop diameter, and R_c is the mode radius of the distribution. The following modified gamma distribution parameters were used to generate the 10,000 profile training data set:

- R_c varied from 0.5 to 200 micrometers,
- LWC from 0.001 to 2 g/m^3,
- γ from 0.3 to 1.8,
- and α from 0.1 to 4.1.

Also, temperature was assumed to uniformly vary from –15° to +5°C in the Mie scattering and extinction equations [2], used for calculation of radar observed reflectivity profiles. For each profile, a 70% range cell to range cell correlation was assumed in the distribution parameters and temperature.

Neural network performance was evaluated using radar reflectivity and cloud parameters calculated from the aircraft-sampled drop size distributions. The cloud parameters MVD, MZD, and LWC, calculated directly from the measured drop size distributions, were compared with the neural net estimated cloud parameters using the radar reflectivity profiles as inputs. The error was measured two ways: (1) by evaluating the correlation coefficient[1] between actual and estimated cloud parameters and (2) by calculating root mean squared (RMS) error. It was found in the original study that errors in estimating drop size scaled linearly with size, so for MVD and MZD the error was expressed in terms of percentage RMS error relative to drop size (MVD or MZD). The following equations were used to evaluate the RMS error in the neural network estimated LWC, MVD, and MZD:

$$E_{LWC} = \frac{\sqrt{\sum_{i=1}^{N}(LWC - LWC_{NN})^2}}{N} \quad (g/m^3)$$

$$E_{MVD} = 100\frac{\sqrt{\sum_{i=1}^{N}\left(\frac{MVD - MVD_{NN}}{MVD}\right)^2}}{N} \quad (\%)$$

and

$$E_{MZD} = 100\frac{\sqrt{\sum_{i=1}^{N}\left(\frac{MZD - MZD_{NN}}{MZD}\right)^2}}{N} \quad (\%)$$

where *LWC, MVD,* and *MZD* are the cloud parameters calculated from actual drop size distributions; LWC_{NN}, MVD_{NN}, and MZD_{NN} are the neural network estimated cloud parameters; and N is the number of samples considered for the error calculations.

---

[1] The correlation coefficient, ρ_{xy}, of a pair of N element data sets, x and y, is defined according to: $\rho_{xy} = \sum_{i=1}^{N}(x_i - \mu_x)(y_i - \mu_y) \Big/ \sqrt{\sum_{i=1}^{N}(x_i - \mu_x)^2 \sum_{j=1}^{N}(y_j - \mu_y)^2}$, where μ_x and μ_y are the averages of the x and y data sets, respectively.

RESULTS

The performance of the 10-35-95, 10-95, and 10-35 GHz frequency neural network was evaluated for 2 km, 1 km, and 500 m range resolutions and range cell size for the clusters of cloud and precipitation conditions shown in figure 3. As stated previously, it was assumed that the radar signal only contained 1 dB STD error for 1- and 2-km range cell size and 0.5 dB STD error for 0.5 km range cell. Signal-to-noise-ratio effects and distance from radar to cloud were not included in the analysis. First as a reference, in figure 7, results of the synthetic data set are presented for 10-35-95 GHz network using 1 km range resolution and when 1 dB STD error was applied to the simulated reflectivity profiles. The results of the NASA data set are presented in figures 8-10. The results will illustrate the strengths and weaknesses of the various frequency combinations. It is evident that the approximate magnitude of the errors in the cloud parameters estimated from the real (NASA) data set is similar to the errors in the synthetic parameters, indicating that the synthetic drop size distributions used to train the net adequately represent real world conditions.

LWC: For the majority of cases tested the neural net estimated LWC values are accurate to within about 0.1 g/m^3. The accuracy of the estimated LWC is even better when 95 GHz data is included, confirming the sensitivity of 95 GHz reflectivity gradient to LWC. It is expected, however, that this same attenuation that makes 95 GHz radar sensitive to LWC will rapidly degrade the sensitivity of the 95 GHz measurements with increasing range, making it ineffective beyond about 10 km. The 10-35 GHz frequency combination should have better long range capability, but the lack of sensitivity to LWC will make it less accurate and suitable for only coarse spatial resolution (1 km +) measurements.

Drop Size Estimation: The errors in the estimated MZD using any of the three frequency combinations (10-35, 10-95, and 10-35-95 GHz) remain below about 100 microns g/m^3 and improve with smaller drop sizes, while MVD errors are slightly worse—about 200 microns. This is not surprising, since the X-band radar measured reflectivity is, in most conditions, proportional to the 6^{th} moment of the drop size distributions and, consequently, better correlated with MZD than MVD. Actually, the results raise the question whether the technique is sufficiently precise to estimate the difference between MZD and MVD. This lack of ability to estimate more than one size parameter is evident in the opposing signs of the estimation errors of MVD and MZD. It appears that the net estimates a size parameter somewhere smaller than the 6^{th} moment, causing a small error most noticeable for small, Rayleigh particles and broad spectral widths. The presence of ice particles in clouds and precipitation affects radar reflectivity and may affect the results of the analysis, since the ice particles were not included in the cloud and precipitation clusters evaluated.

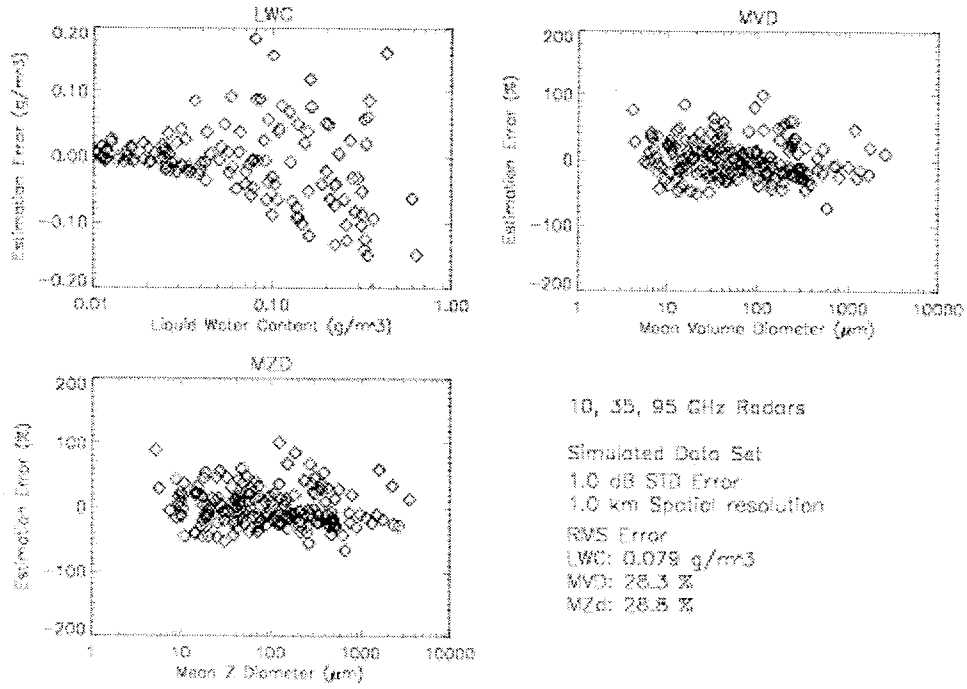

FIGURE 7. NEURAL NET ESTIMATION ERROR (NEURAL NET ESTIMATED—SIMULATED QUANTITY) FOR THE 10-35-95 GHz FREQUENCY COMBINATION USING SIMULATED DATA POINTS

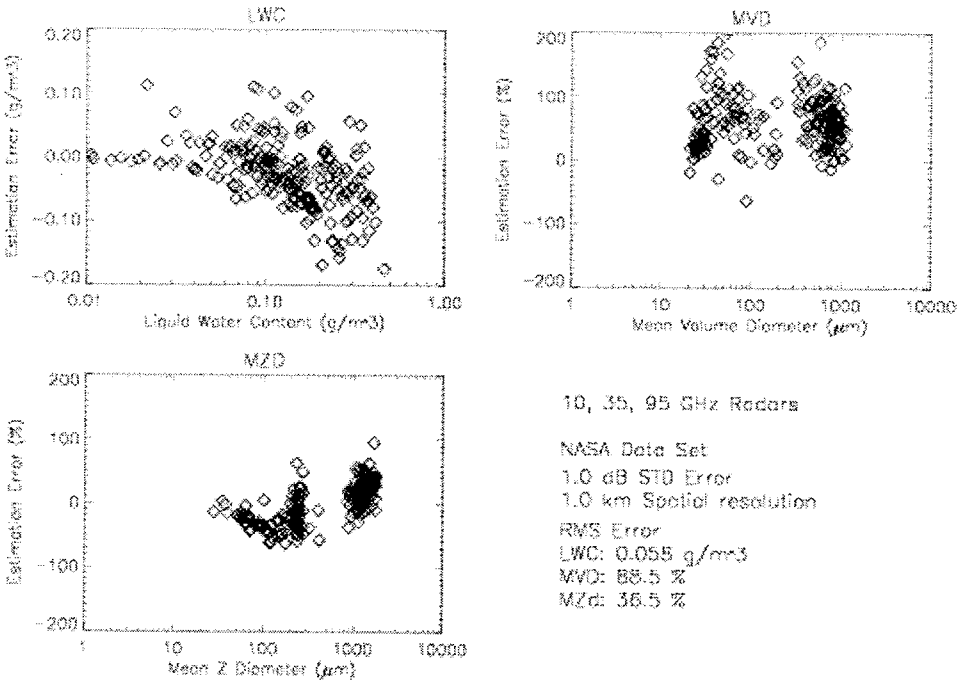

FIGURE 8. NEURAL NET ESTIMATION ERROR (NEURAL NET ESTIMATED—AIRCRAFT-SAMPLED QUANTITY) FOR THE 10-35-95 GHz FREQUENCY COMBINATION USING ALL THE NASA DATA POINTS

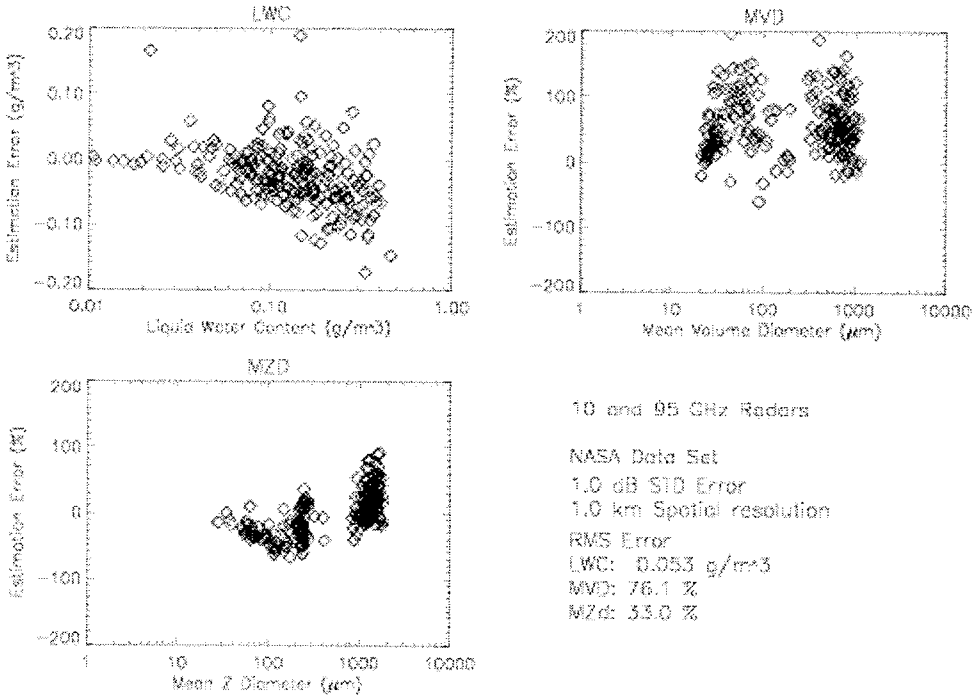

FIGURE 9. NEURAL NET ESTIMATION ERROR (NEURAL NET ESTIMATED—AIRCRAFT-SAMPLED QUANTITY) FOR THE 10-95 GHz FREQUENCY COMBINATION USING ALL OF THE NASA DATA POINTS

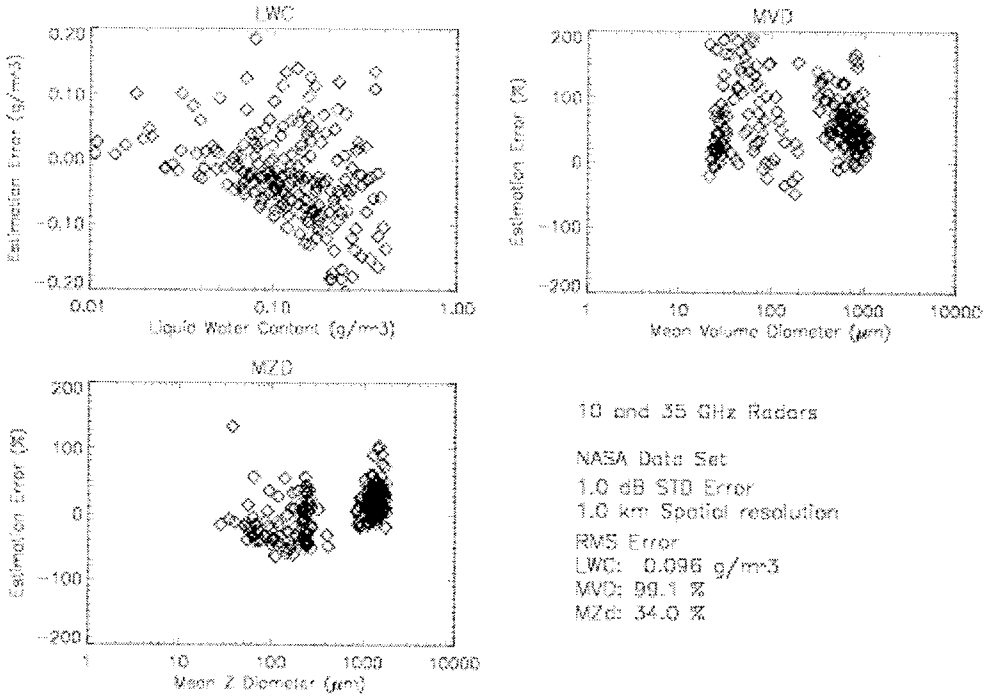

FIGURE 10. NEURAL NET ESTIMATION ERROR (NEURAL NET ESTIMATED—AIRCRAFT-SAMPLED QUANTITY) FOR THE 10-35 GHz FREQUENCY COMBINATION USING ALL OF THE NASA DATA POINTS

The results of all the tested frequency combinations, range resolutions, and cloud and precipitation conditions are summarized in tables 1, 2, 3, and 4. Scatter plots corresponding to each entry in the tables are provided in appendix A (the scatter plots may actually be better indicators of algorithm performance than the table entries).

TABLE 1. ERROR OF THE NEURAL NET ESTIMATED PARAMETERS FOR ALL DATA POINTS

		Error (All Data)		
		10-95 GHz	10-35-95 GHz	10-35 GHz
2-km Range Resolution	LWC g/m^3	0.05	0.05	0.06
	MVD %	75	69	78
	MZD %	26	28	23
1-km Range Resolution	LWC	0.05	0.06	0.10
	MVD	76	89	99
	MZD	33	37	34
0.5-km Range Resolution	LWC	0.08	0.08	0.09
	MVD	87	92	97
	MZD	26	32	25

TABLE 2. ERROR OF THE NEURAL NET ESTIMATED PARAMETERS FOR SMALL DROPS AND LOW LWC

		Error (Small Drops and Low LWC)		
		10-95 GHz	10-35-95 GHz	10-35 GHz
2-km Range Resolution	LWC g/m^3	0.04	0.03	0.06
	MVD %	53	93	63
	MZD %	18	33	15
1-km Range Resolution	LWC	0.04	0.05	0.07
	MVD	49	121	66
	MZD	17	50	17
0.5-km Range Resolution	LWC	0.05	0.04	0.06
	MVD	63	116	75
	MZD	15	33	17

TABLE 3. ERROR OF THE NEURAL NET ESTIMATED PARAMETERS FOR LARGE DROPS

		Error (Large Drops)		
		10-95 GHz	10-35-95 GHz	10-35 GHz
2-km Range Resolution	LWC g/m^3	0.05	0.05	0.05
	MVD %	42	58	30
	MZD %	14	22	10
1-km Range Resolution	LWC	0.05	0.06	0.07
	MVD	51	73	51
	MZD	24	29	24
0.5-km Range Resolution	LWC	0.09	0.09	0.06
	MVD	51	85	27
	MZD	17	32	12

TABLE 4. ERROR OF THE NEURAL NET ESTIMATED PARAMETERS FOR SMALL DROPS AND HIGH LWC

		Error (Small Drops and High LWC)		
		10-95 GHz	10-35-95 GHz	10-35 GHz
2-km Range Resolution	LWC g/m^3	0.07	0.06	0.09
	MVD %	32	58	36
	MZD %	12	33	14
1-km Range Resolution	LWC	0.07	0.07	0.16
	MVD	28	74	54
	MZD	16	33	17
0.5-km Range Resolution	LWC	0.08	0.07	0.17
	MVD	31	73	55
	MZD	13	30	14

CONCLUSIONS

Results indicate that the multifrequency technique, in combination with the artificial neural network processing algorithm, can estimate LWC, MVD, and MZD with fair accuracy in a wide variety of liquid cloud and precipitation conditions. The synthetic cloud and precipitation model used to train the neural network may be an adequate representation of real world conditions, since the algorithm gave fair performance even in bimodal drop size conditions.

While MVD and MZD can be estimated at similar accuracy using any of the three (10-35, 10-95, or 10-35-95 GHz) radar combinations, only the 10-95 or 10-35-95 GHz frequency combinations can be used to estimate LWC consistently.

The multifrequency technique is not as well suited to measure the size parameter MVD as MZD, which is more strongly affected by the largest drops that dominate reflectivity. Neither of these parameters are necessarily correlated with the more conventional MVD, particularly for bimodal drop size distributions. The MVD behaved very erratically for the bimodal distributions analyzed.

The results also indicate that in small (Rayleigh) drop size and high LWC conditions, the 10-35-95 or 10-95 GHz radar combinations can effectively estimate LWC, MVD, and MZD at finer than 1-km range resolution. The potential benefit of this capability is that in the most hazardous conditions, an operational system will be able to provide pilots and ground crew more resolved maps of the spatial extent and intensity of icing potential.

REFERENCES

1. Quadrant Engineering Inc., "Evaluation of Technologies for the Design of a Prototype In-Flight Remote Aircraft Icing Potential Detection System," *Final R&D Report*, Contract No. DACA39-97-M-1476, p. 85, 1998.

2. Ulaby, F.T., R.K. More, and A.K. Fung, *Microwave Remote Sensing, Active and Passive,* Volume 1, Addison Wesley, Reading, Mass., pp. 456.

3. Zell et al., 1995, "Stuttgart Neural Network Simulator User Manual," *User Manual,* Version 4.1, University of Stuttgart, Germany, Report number 6/95, pp. 308, 1995.

GLOSSARY

Drop Size Distribution—The measured or modeled distribution of drop diameters for clouds or rain. Units are number of drops per meter per cubic meter or m^{-4}.

Liquid Water Content (LWC)—The water content, in grams per cubic meter, of the liquid portion of the cloud or precipitation.

Mean Volume Diameter (MVD)—Particle diameter corresponding to the mean of the volume distribution. Volume distribution is computed from the given drop size (diameter) distribution. Note that median volume diameter (denoted MeVD in this report) is a much more commonly used icing variable.

Median Volume Diameter (MeVD)—Particle diameter corresponding to the median of volume distribution. This is usually denoted by MVD in the icing literature.

Mean Z Diameter (MZD)—Particle diameter corresponding to mean cloud reflectivity.

Mie Scattering—Mie scattering refers to the complete solution for electromagnetic scattering from dielectric spheres as computed by G. Mie in 1908. This relatively complicated formulation is required when the particle size is within an order of magnitude of the electromagnetic wavelength. Approximate formulas are often used in the optical limit ($d>>\lambda$) and Rayleigh limit ($d<<\lambda$) to simplify calculations.

Multiparameter Radar—Radar system capable of measuring a variety of parameters at one or more frequencies. For a meteorological radar, these parameters include cloud reflectivity, Doppler spectrum of the scattered signal (or its moments), and four additional polarimetric parameters, including linear depolarization ratio LDR, differential reflectivity Z_{dr}, and the magnitude and phase of the copolarized correlation coefficient, ρ_{hv}.

Neural Network—A software algorithm used to determine output parameters based on a network of interconnected summing nodes with nonlinear response to the input. The neural network was originally developed to imitate the function of interconnected brain neurons. The basic building block of neural networks are nonlinear summing nodes that are coupled to other nodes through connections with variable weighting factors. These weighting factors, along with the transfer function of the summing nodes, are adjusted to minimize estimation errors by using a set of known input and output vectors.

Rayleigh Scattering—Simplified scattering regime for particles much smaller than the electromagnetic wavelength. For larger particles, on the order of the radar wavelength, the complete Mie solution must be computed. Scattering from particles much larger than the electromagnetic wavelength can be approximated using optical limit formulas.

Reflectivity, *Z*—Frequency-independent parameter equal to the sixth moment of drop size distribution. Reflectivity is proportional to backscattered power. The sixth moment arises from the fact that the radar cross section of a small particle ($d<<\lambda$) is proportional to the sixth power of particle diameter. Reflectivity is typically expressed on a decibel scale as *dBZ*, which equals $10\log_{10}(Z)$.

APPENDIX A—SUPPORTING DATA SCATTER PLOTS

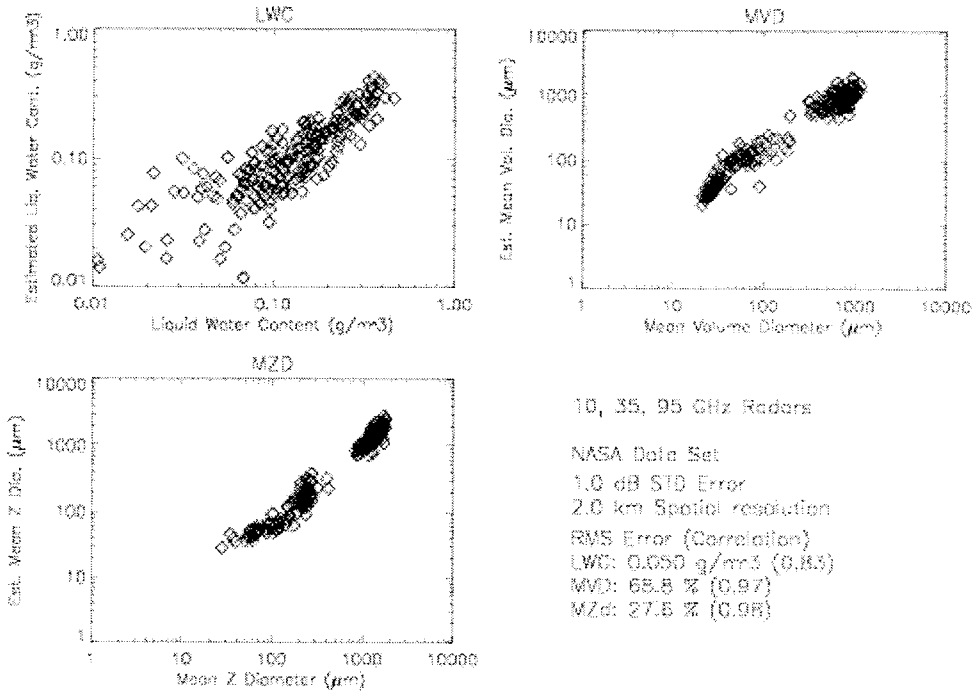

FIGURE A-1. 10-35-95 GHz RADARS, 2-km RANGE RESOLUTION, 1-dB STD MEASUREMENT NOISE, ALL DATA

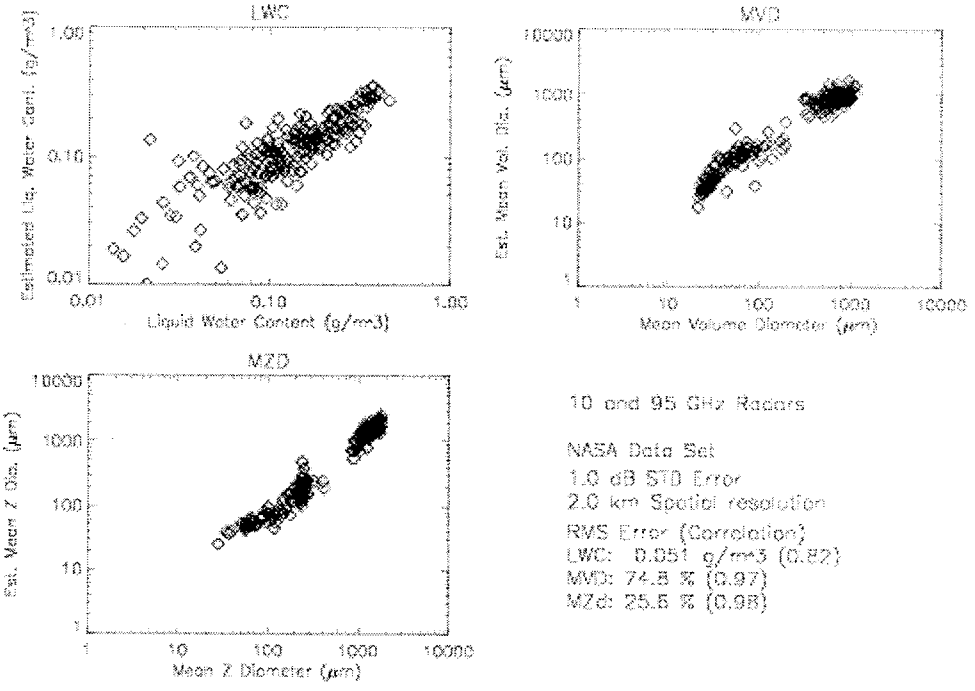

FIGURE A-2. 10-95 GHz RADARS, 2-km RANGE RESOLUTION, 1-dB STD MEASUREMENT NOISE, ALL DATA

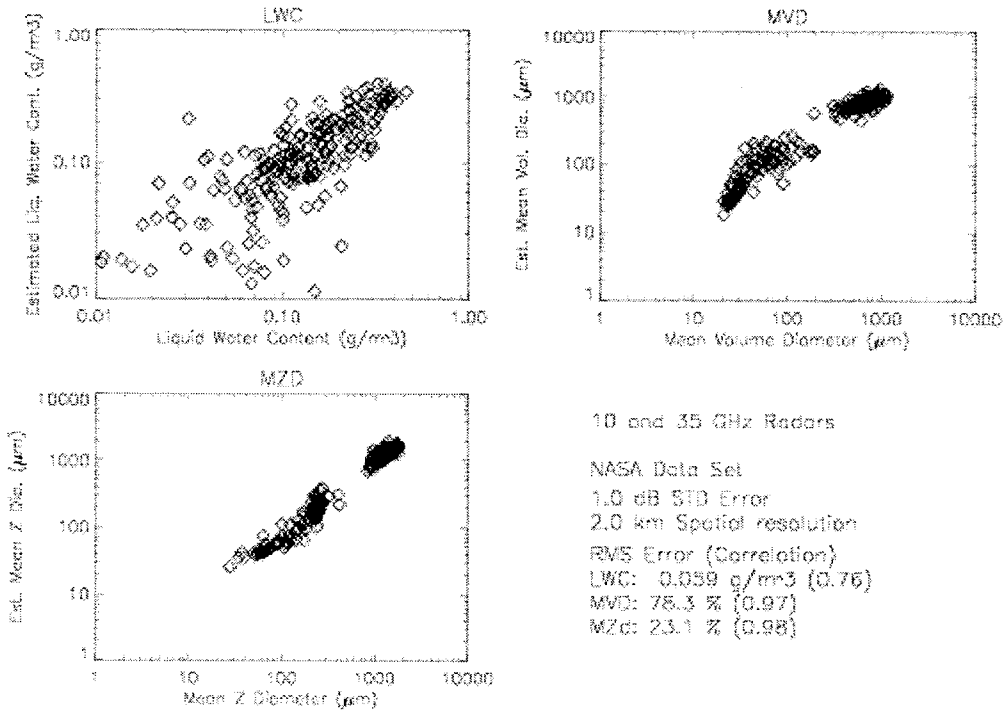

FIGURE A-3. 10-35 GHz RADARS, 2-km RANGE RESOLUTION, 1-dB STD MEASUREMENT NOISE, ALL DATA

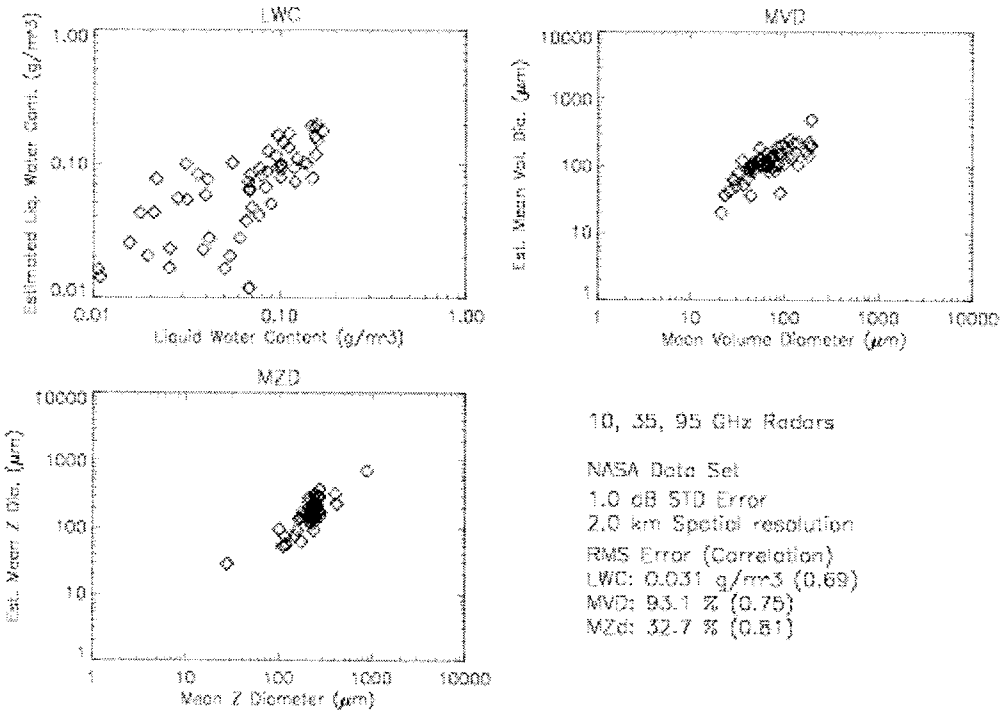

FIGURE A-4. 10-35-95 GHz RADARS, 2-km RANGE RESOLUTION, 1-dB STD MEASUREMENT NOISE, SMALL DROPS AND LOW LWC

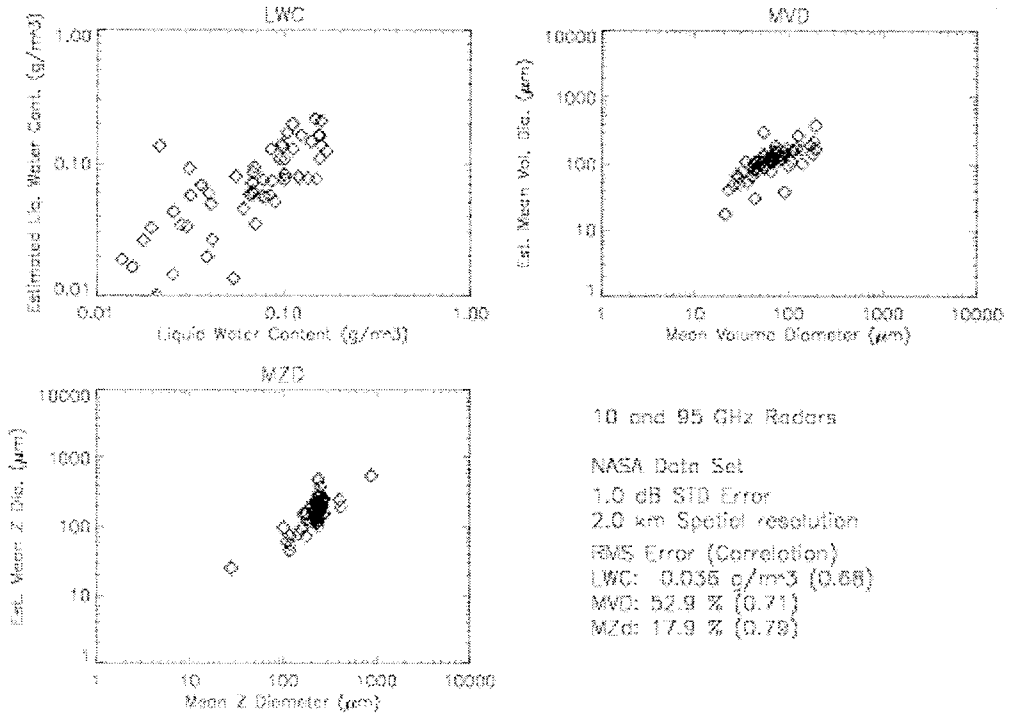

FIGURE A-5. 10-95 GHz RADARS, 2-km RANGE RESOLUTION, 1-dB STD MEASUREMENT NOISE, SMALL DROPS AND LOW LWC

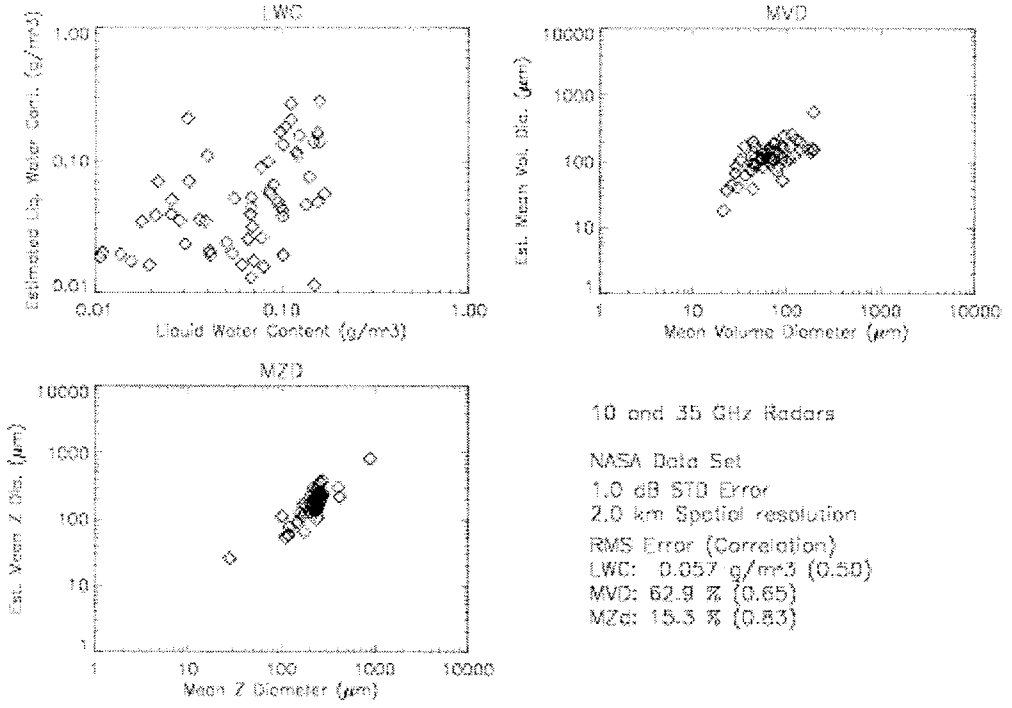

FIGURE A-6. 10-35 GHz RADARS, 2-km RANGE RESOLUTION, 1-dB STD MEASUREMENT NOISE, SMALL DROPS AND LOW LWC

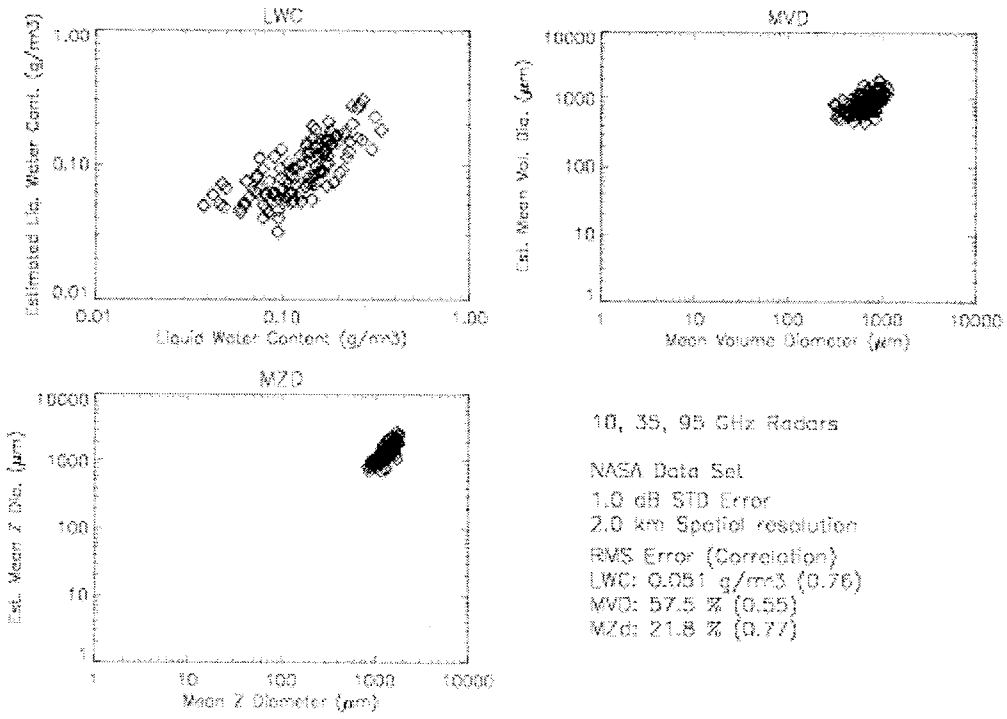

FIGURE A-7. 10-35-95 GHz RADARS, 2-km RANGE RESOLUTION, 1-dB STD MEASUREMENT NOISE, LARGE DROPS

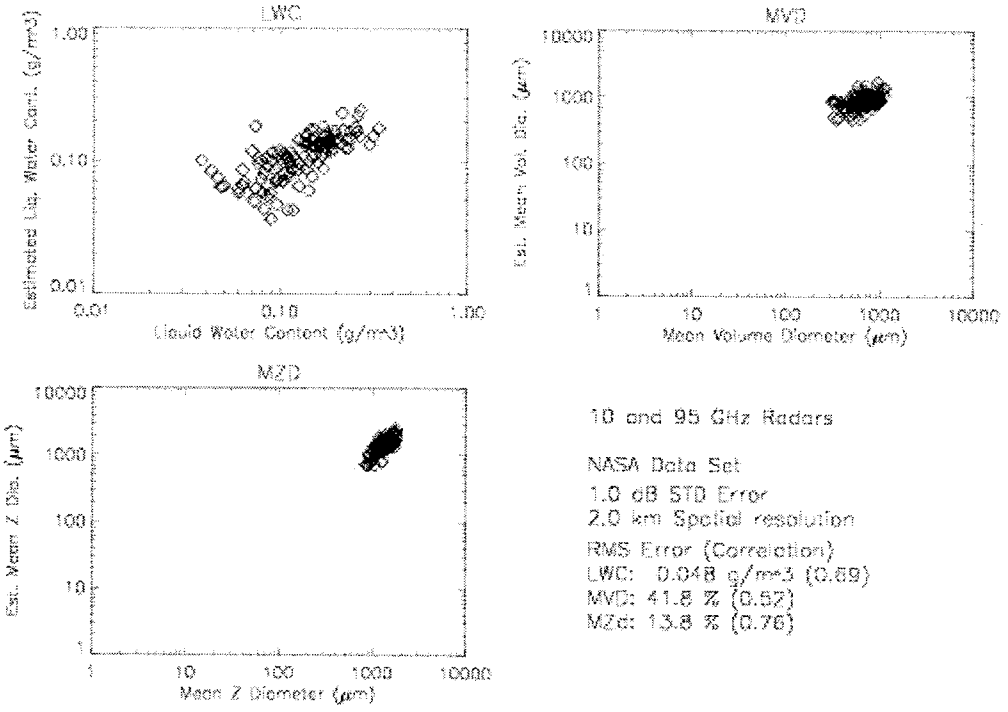

FIGURE A-8. 10-95 GHz RADARS, 2-km RANGE RESOLUTION, 1-dB STD MEASUREMENT NOISE, LARGE DROPS

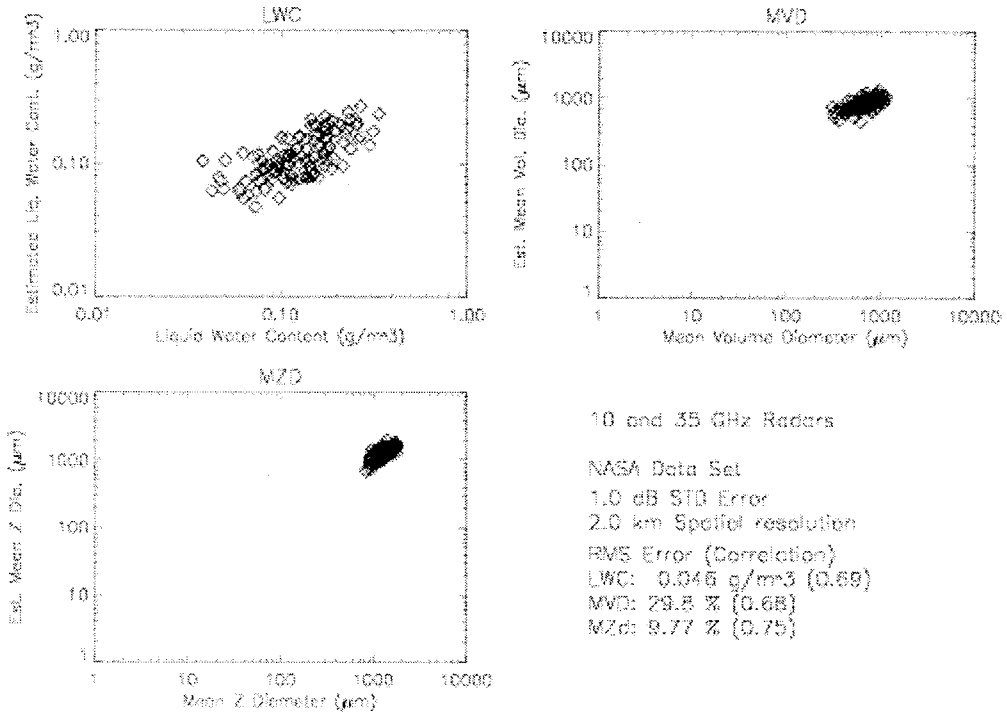

FIGURE A-9. 10-35 GHz RADARS, 2-km RANGE RESOLUTION, 1-dB STD MEASUREMENT NOISE, LARGE DROPS

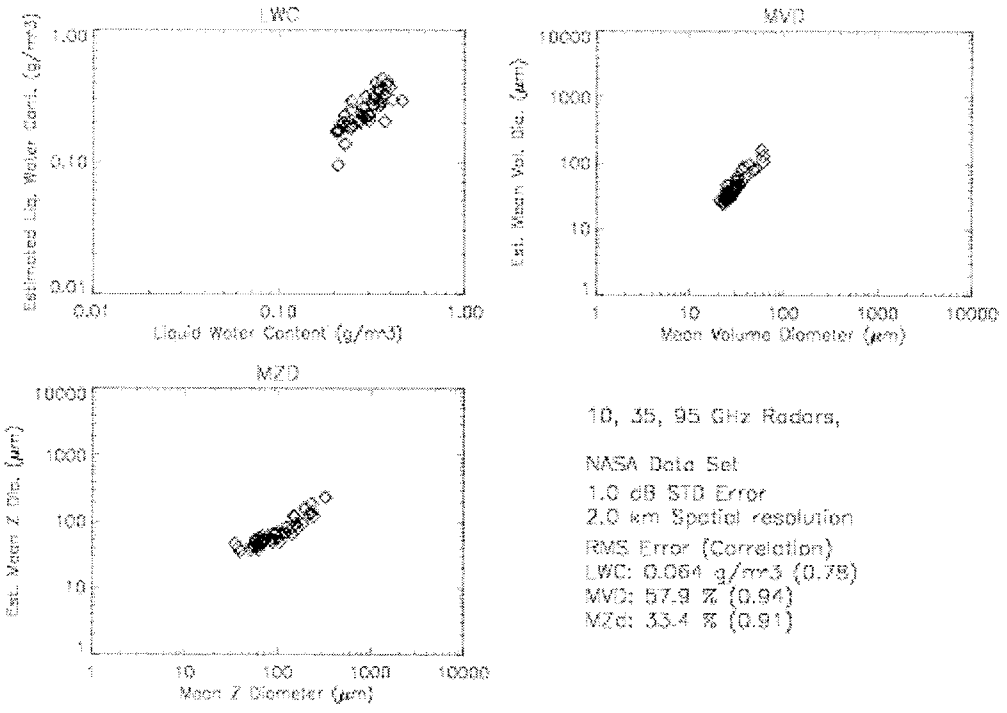

FIGURE A-10. 10-35-95 GHz RADARS, 2-km RANGE RESOLUTION, 1-dB STD MEASUREMENT NOISE, SMALL DROPS AND HIGH LWC

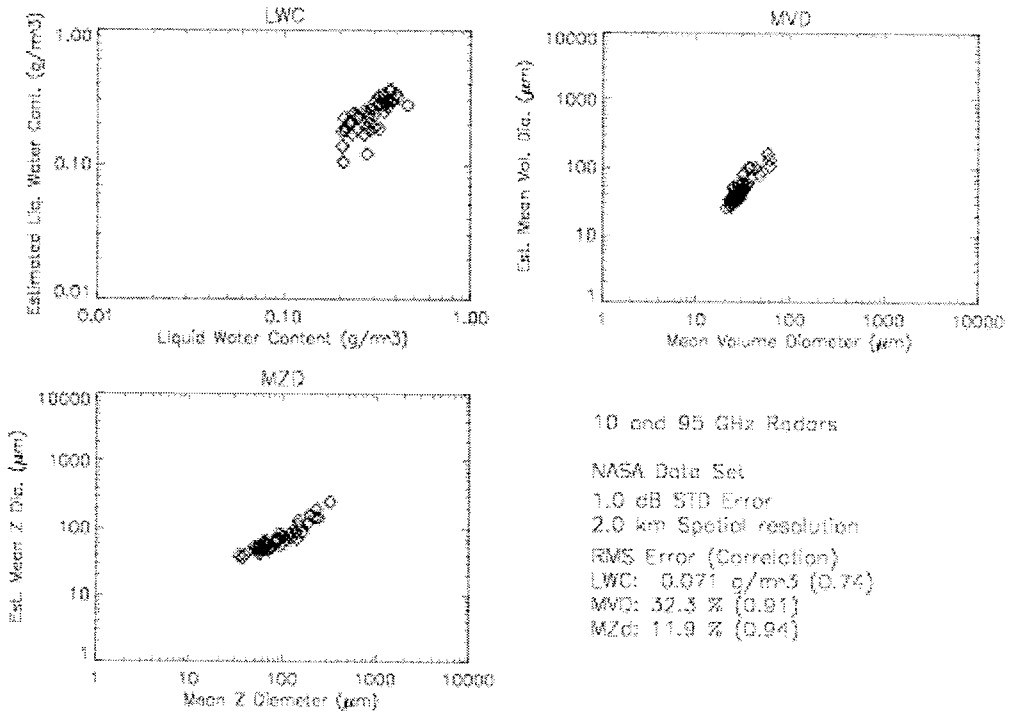

FIGURE A-11. 10-95 GHz RADARS, 2-km RANGE RESOLUTION, 1-dB STD MEASUREMENT NOISE, SMALL DROPS AND HIGH LWC

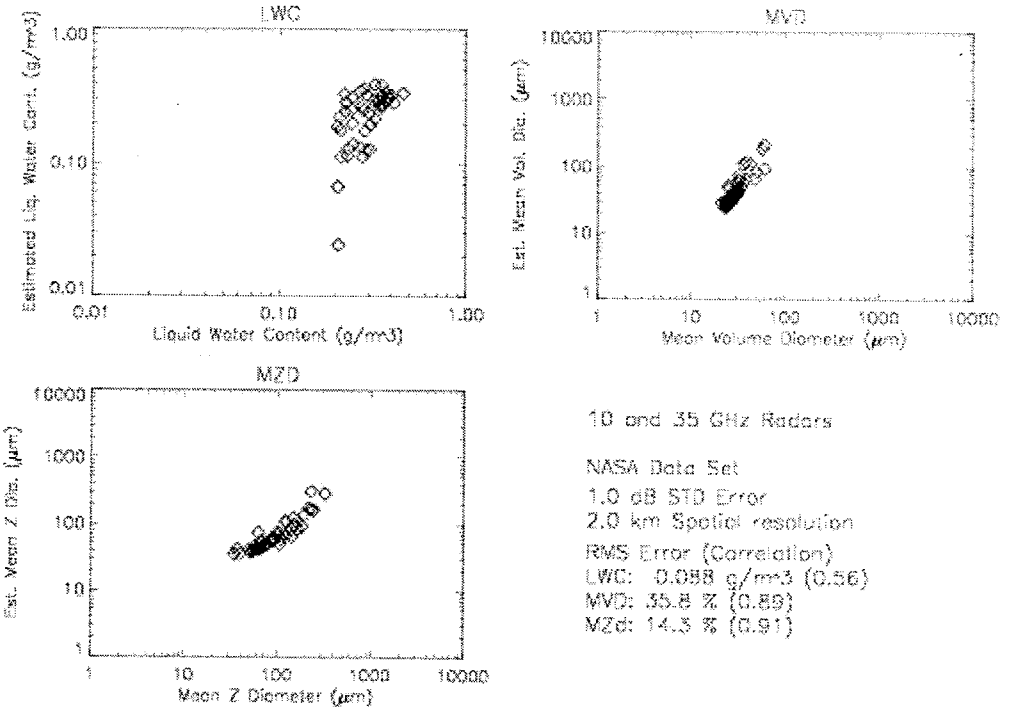

FIGURE A-12. 10-35 GHz RADARS, 2-km RANGE RESOLUTION, 1-dB STD MEASUREMENT NOISE, SMALL DROPS AND HIGH LWC

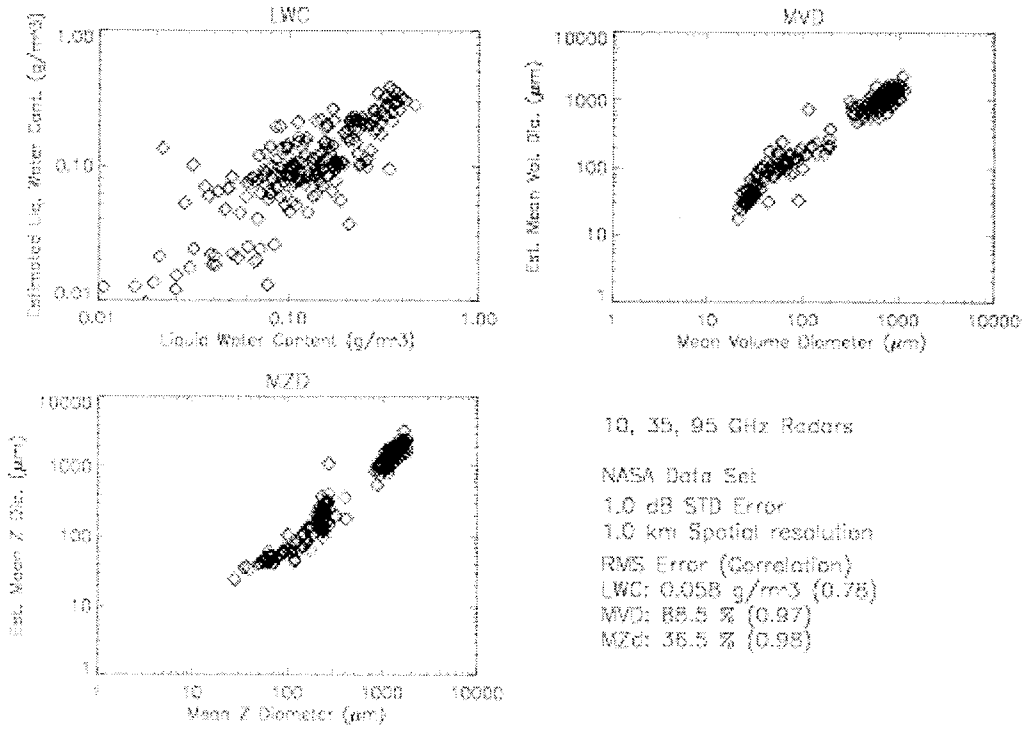

FIGURE A-13. 10-35-95 GHz RADARS, 1-km RANGE RESOLUTION, 1-dB STD MEASUREMENT NOISE, ALL DATA

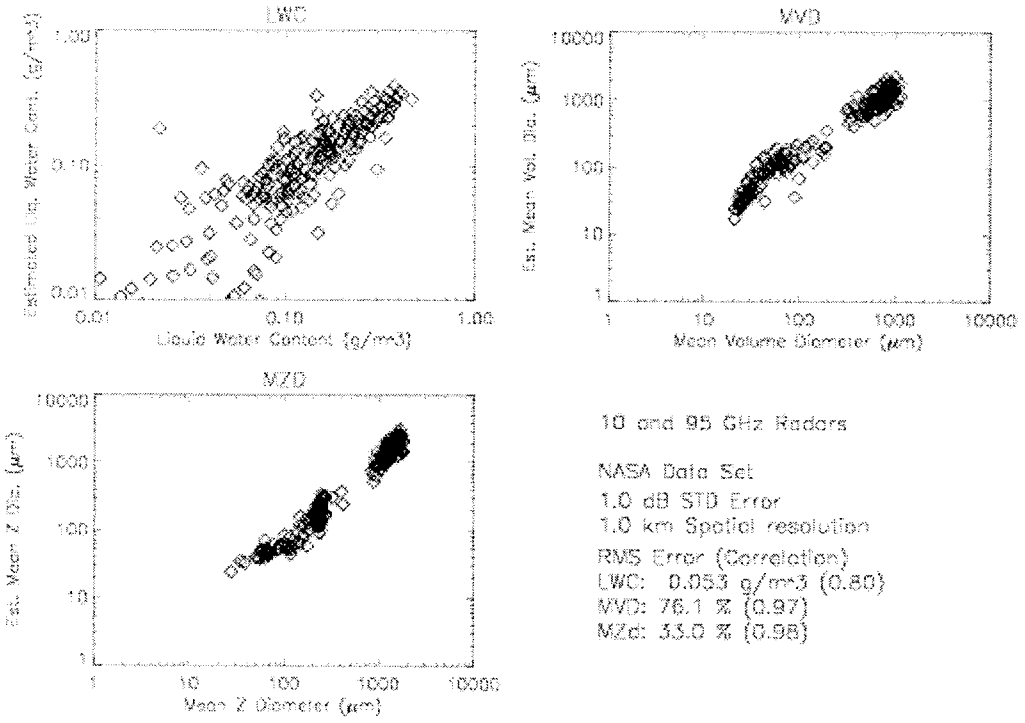

FIGURE A-14. 10-95 GHz RADARS, 1-km RANGE RESOLUTION, 1-dB STD MEASUREMENT NOISE, ALL DATA

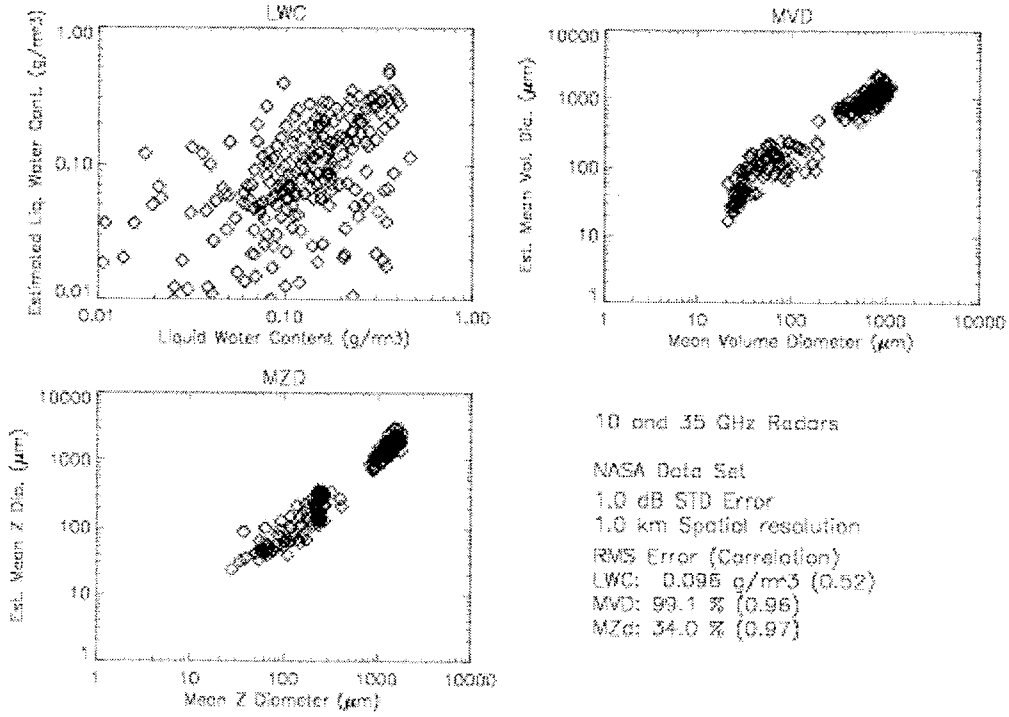

FIGURE A-15. 10-35 GHz RADARS, 1-km RANGE RESOLUTION, 1-dB STD MEASUREMENT NOISE, ALL DATA

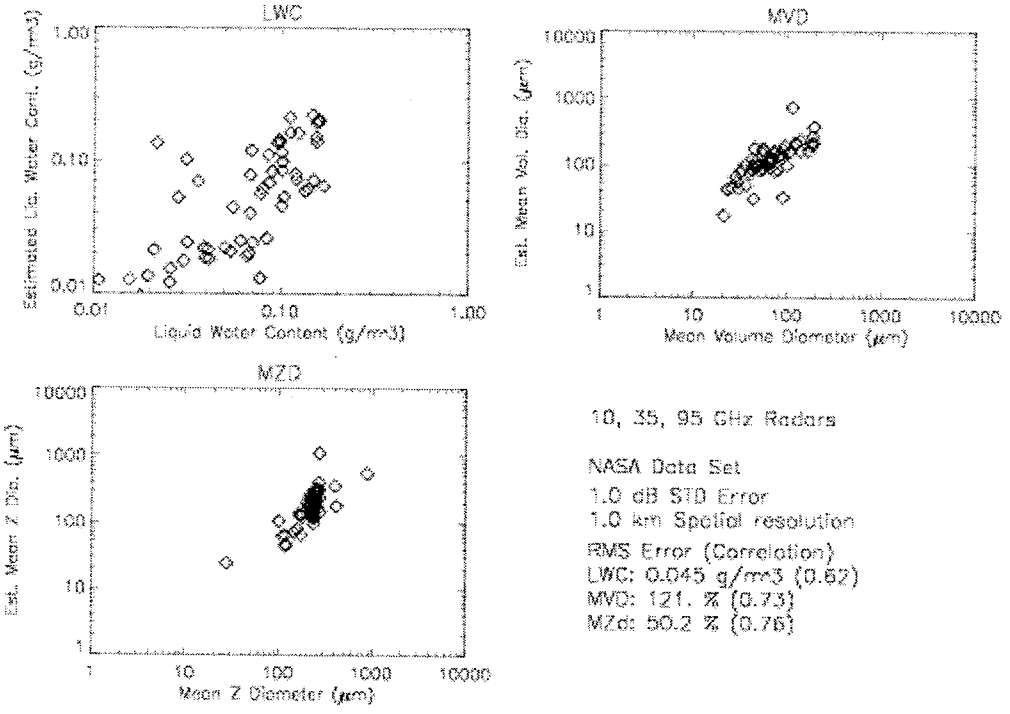

FIGURE A-16. 10-35-95 GHz RADARS, 1-km RANGE RESOLUTION, 1-dB STD MEASUREMENT NOISE, SMALL DROPS AND LOW LWC

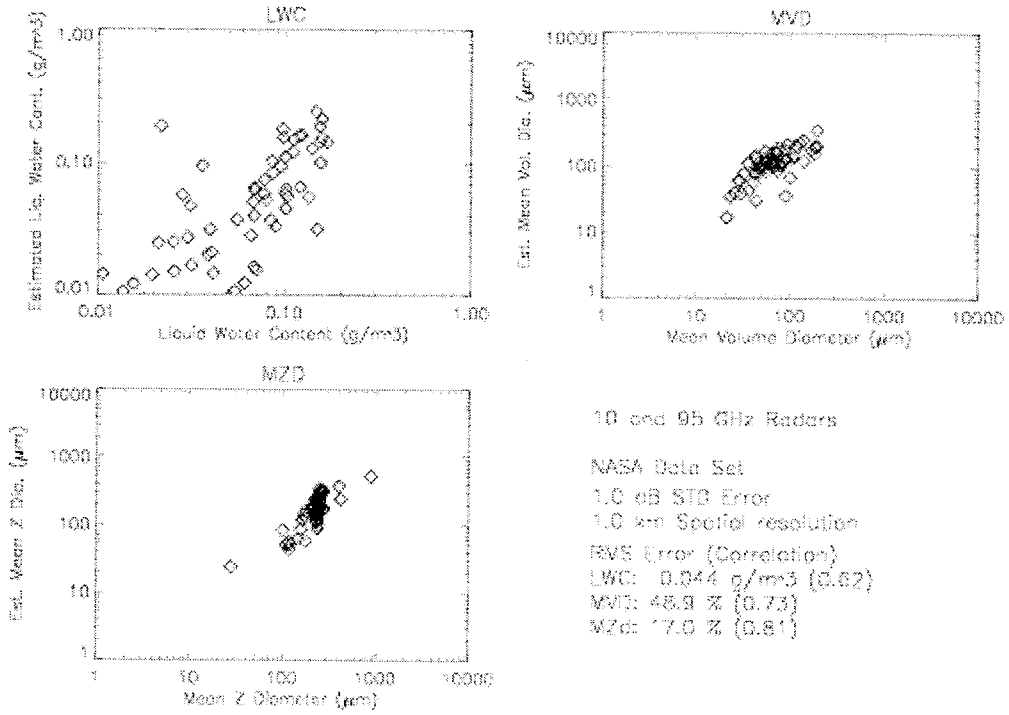

FIGURE A-17. 10-95 GHz RADARS, 1-km RANGE RESOLUTION, 1-dB STD MEASUREMENT NOISE, SMALL DROPS AND LOW LWC

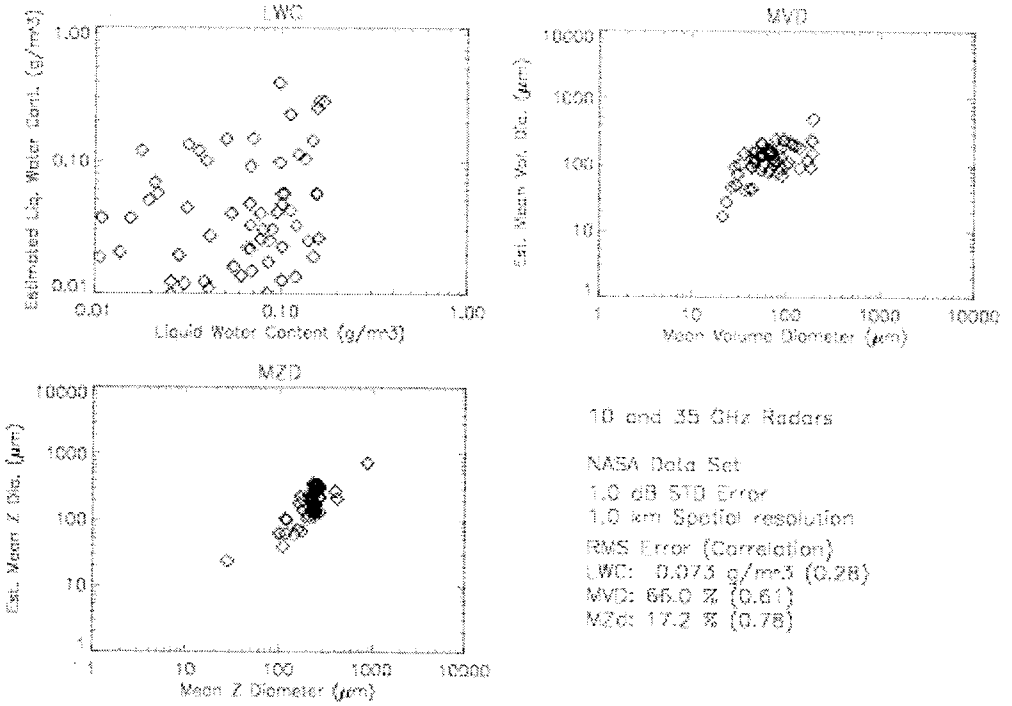

FIGURE A-18. 10-35 GHz RADARS, 1-km RANGE RESOLUTION, 1-dB STD MEASUREMENT NOISE, SMALL DROPS AND LOW LWC

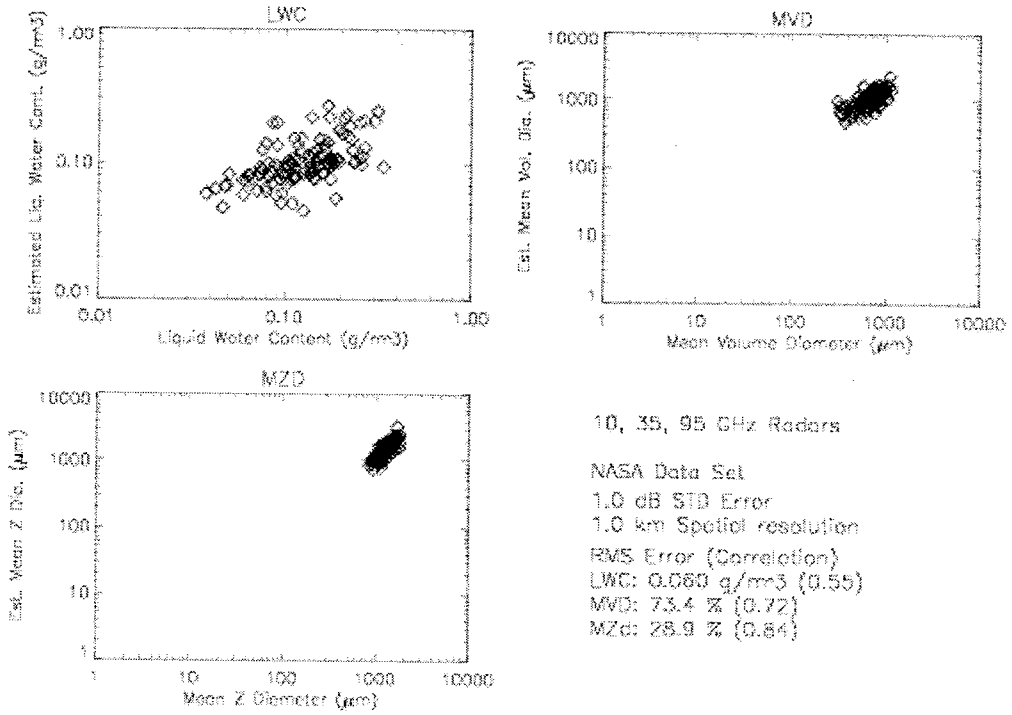

FIGURE A-19. 10-35-95 GHz RADARS, 1-km RANGE RESOLUTION, 1-dB STD MEASUREMENT NOISE, LARGE DROPS

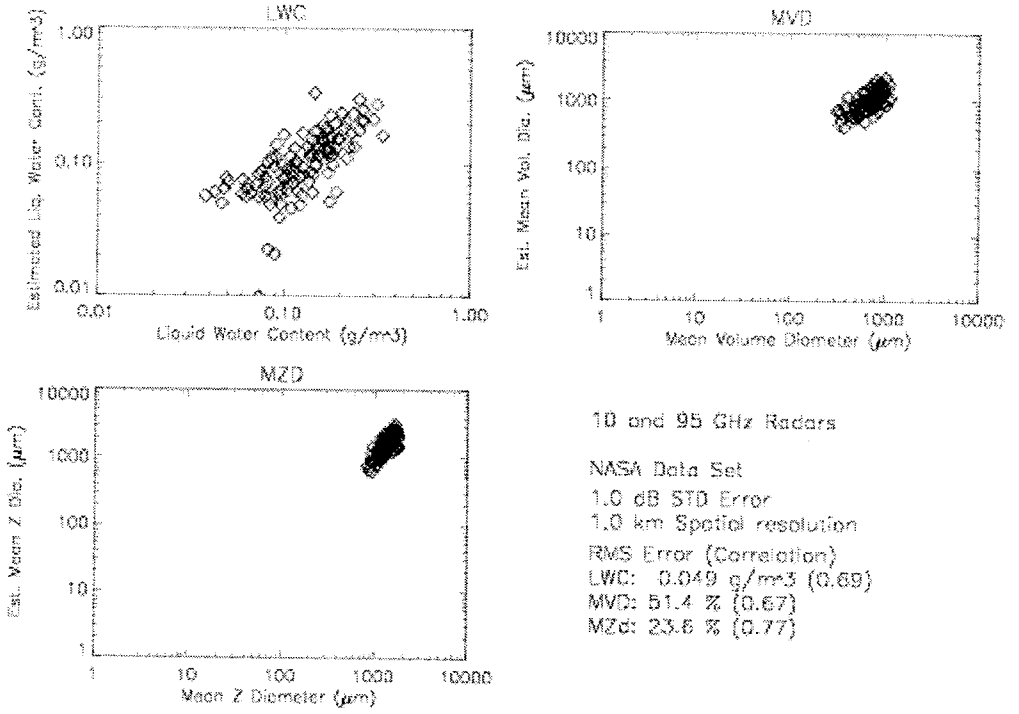

FIGURE A-20. 10-95 GHz RADARS, 1-km RANGE RESOLUTION, 1-dB STD MEASUREMENT NOISE, LARGE DROPS

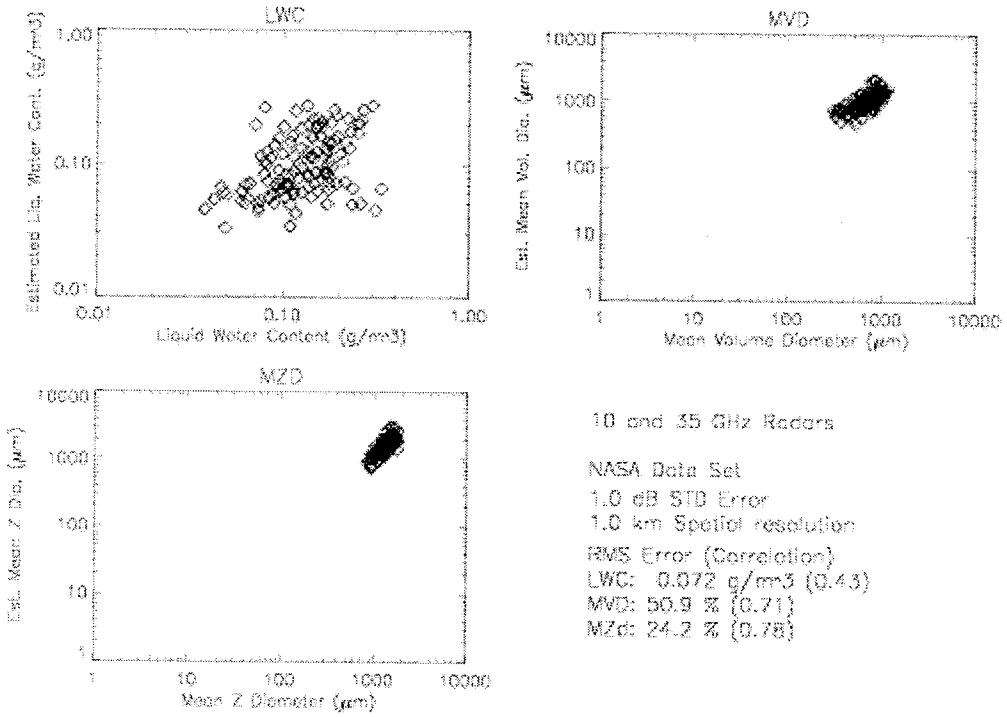

FIGURE A-21. 10-35 GHz RADARS, 1-km RANGE RESOLUTION, 1-dB STD MEASUREMENT NOISE, LARGE DROPS

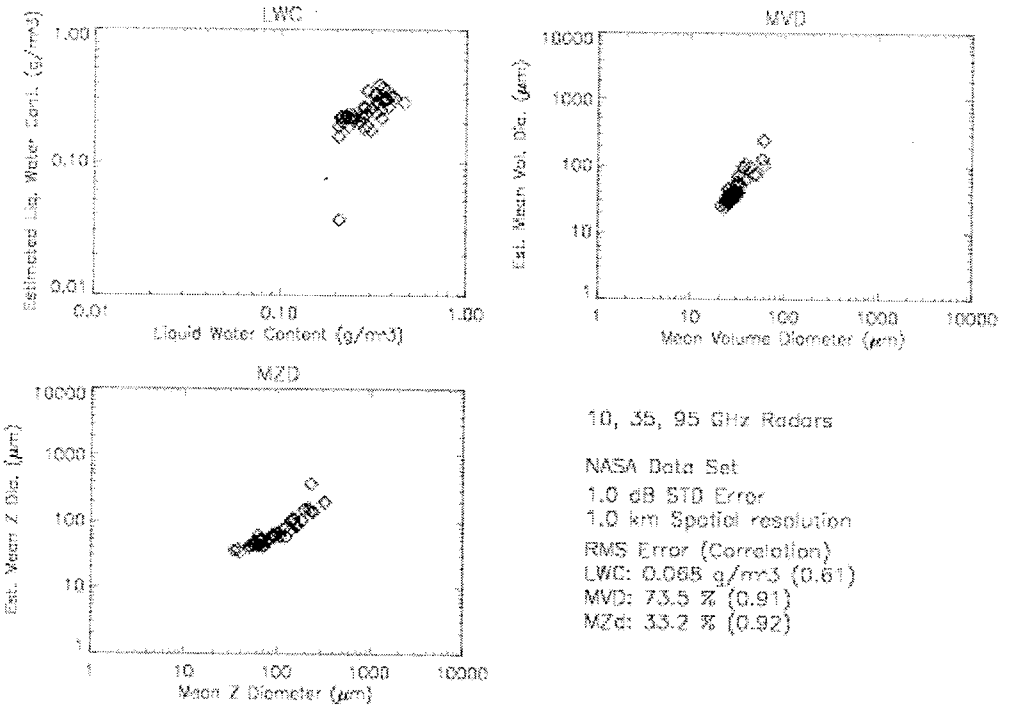

FIGURE A-22. 10-35-95 GHz RADARS, 1-km RANGE RESOLUTION, 1-dB STD MEASUREMENT NOISE, SMALL DROPS AND HIGH LWC

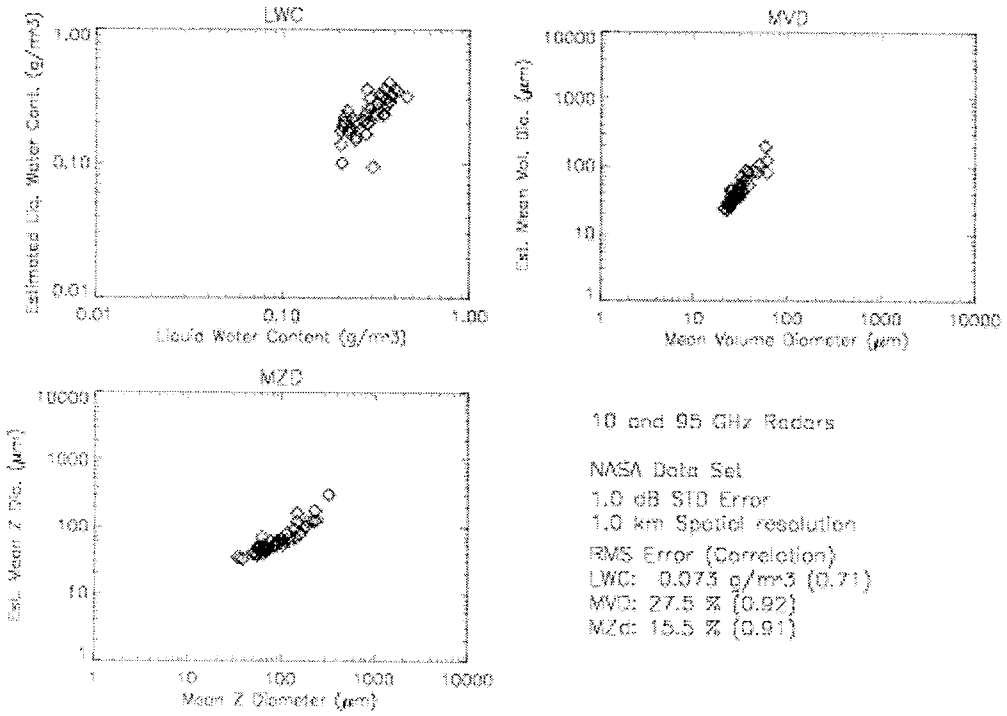

FIGURE A-23. 10-95 GHz RADARS, 1-km RANGE RESOLUTION, 1-dB STD MEASUREMENT NOISE, SMALL DROPS AND HIGH LWC

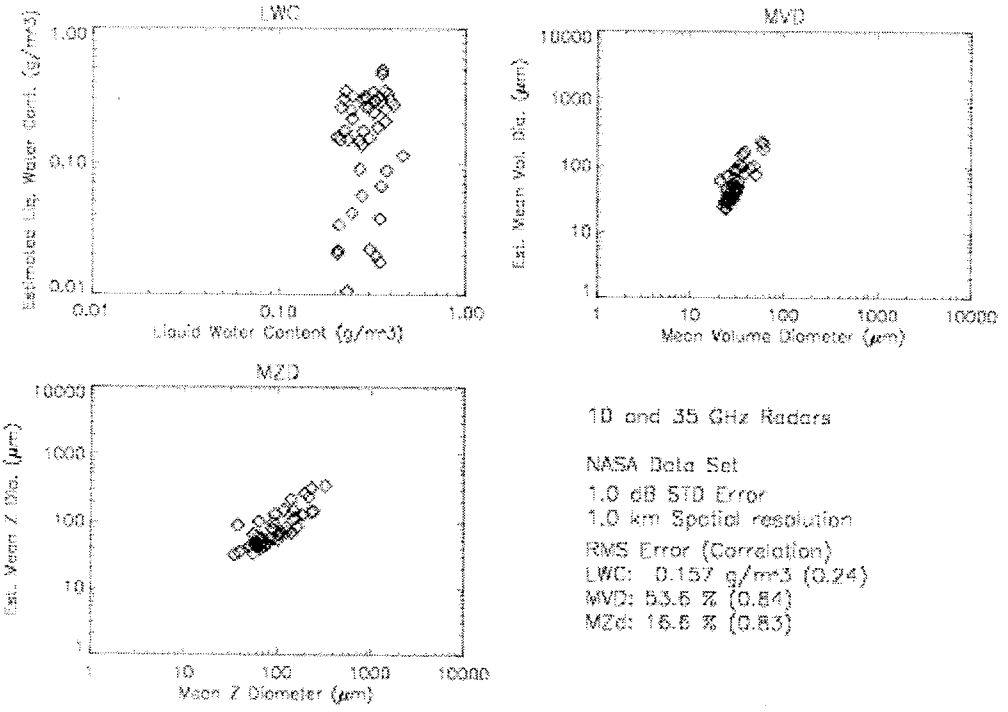

FIGURE A-24. 10-35 GHz RADARS, 1-km RANGE RESOLUTION, 1-dB STD MEASUREMENT NOISE, SMALL DROPS AND HIGH LWC

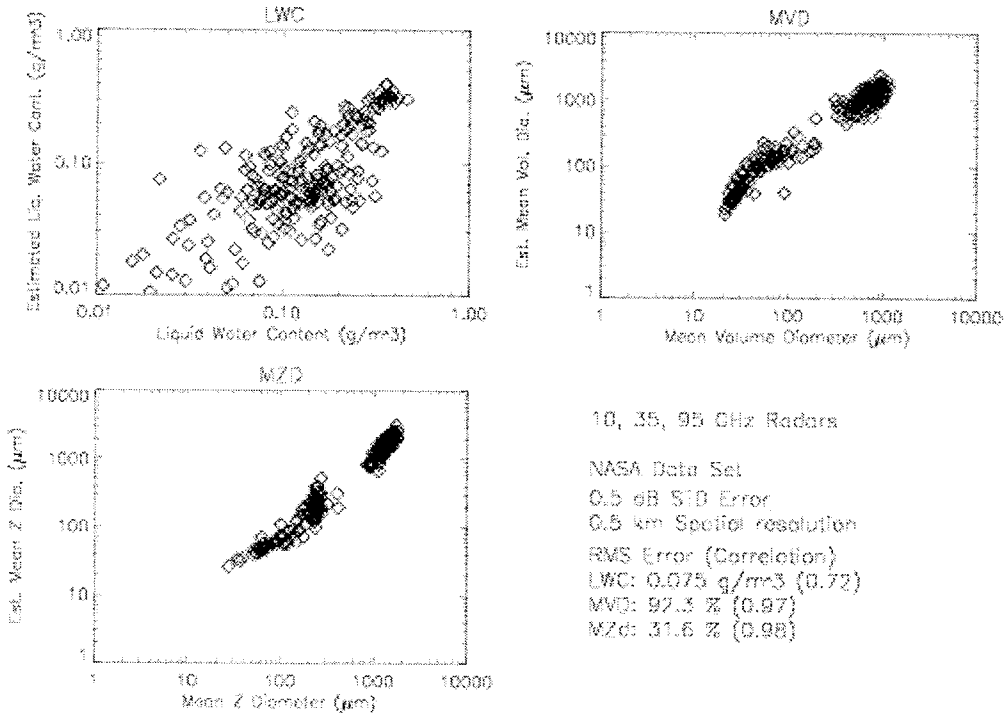

FIGURE A-25. 10-35-95 GHz RADARS, 500-m RANGE RESOLUTION, 0.5-dB STD MEASUREMENT NOISE, ALL DATA

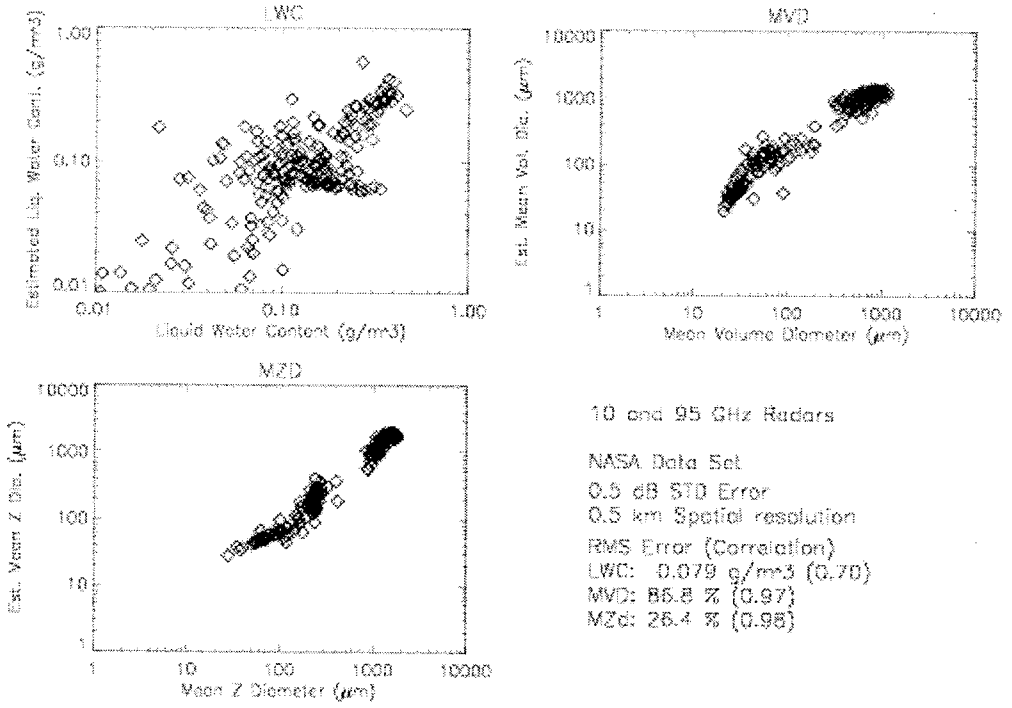

FIGURE A-26. 10-95 GHz RADARS, 500-m RANGE RESOLUTION, 0.5-dB STD MEASUREMENT NOISE, ALL DATA

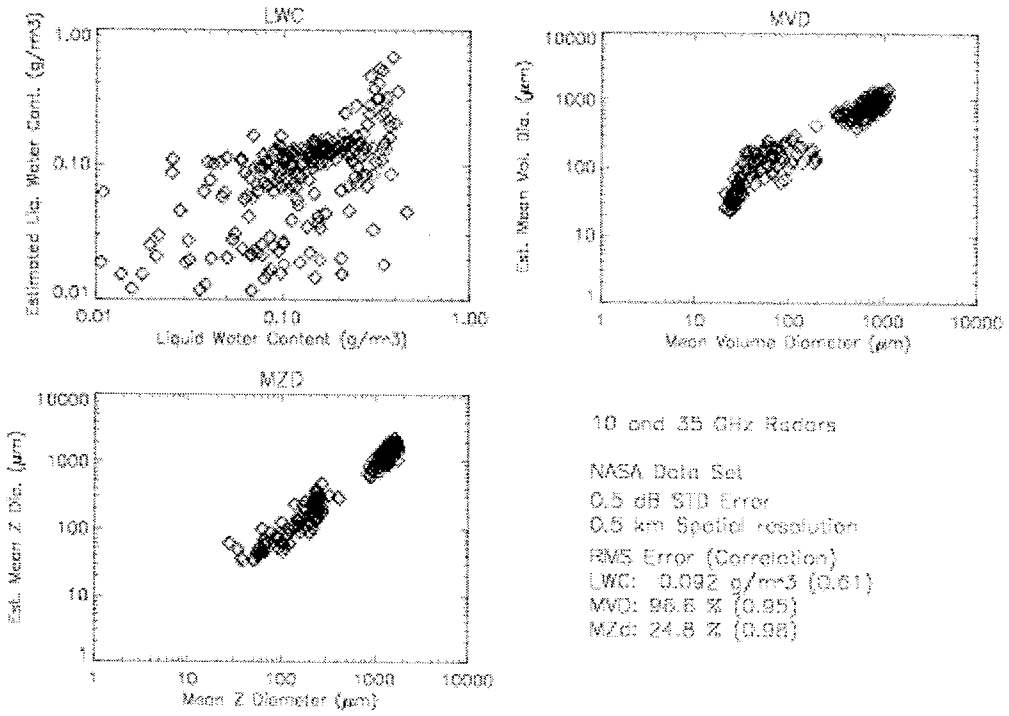

FIGURE A-27. 10-35 GHz RADARS, 500-m RANGE RESOLUTION, 0.5-dB STD MEASUREMENT NOISE, ALL DATA

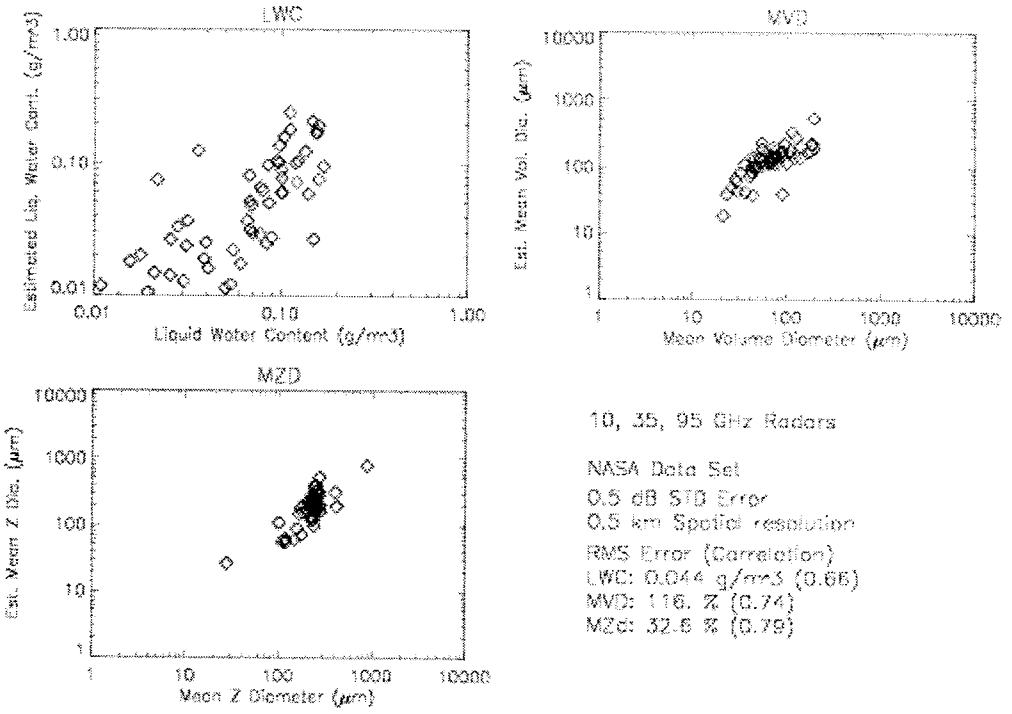

FIGURE A-28. 10-35-95 GHz RADARS, 500-m RANGE RESOLUTION, 0.5-dB STD MEASUREMENT NOISE, SMALL DROPS AND LOW LWC

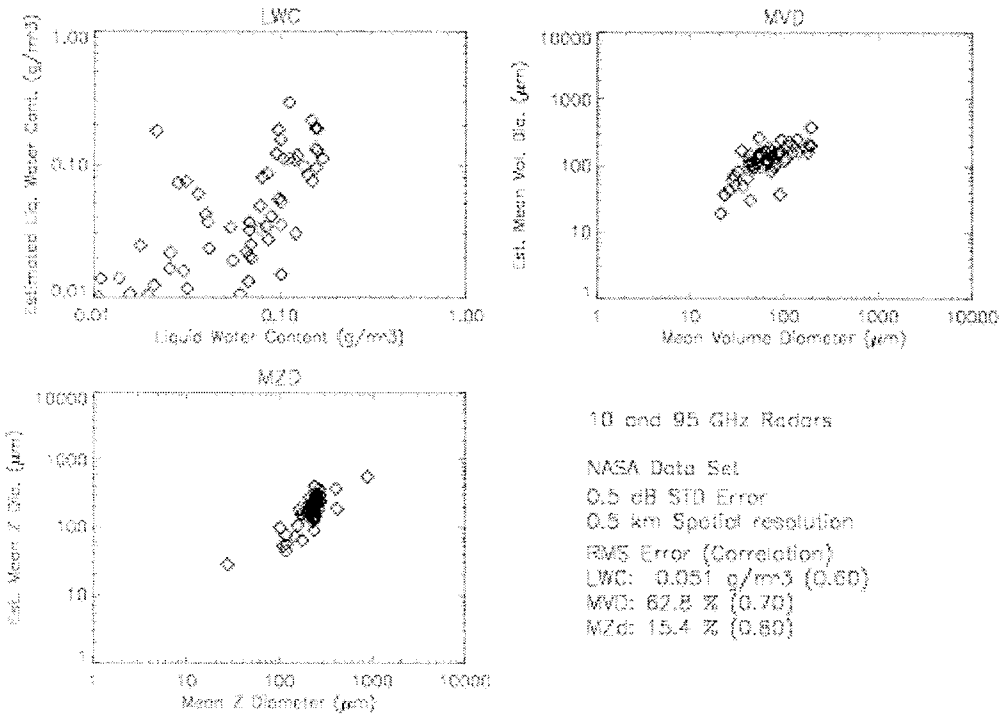

FIGURE A-29. 10-95 GHz RADARS, 500-m RANGE RESOLUTION, 0.5-dB STD MEASUREMENT NOISE, SMALL DROPS AND LOW LWC

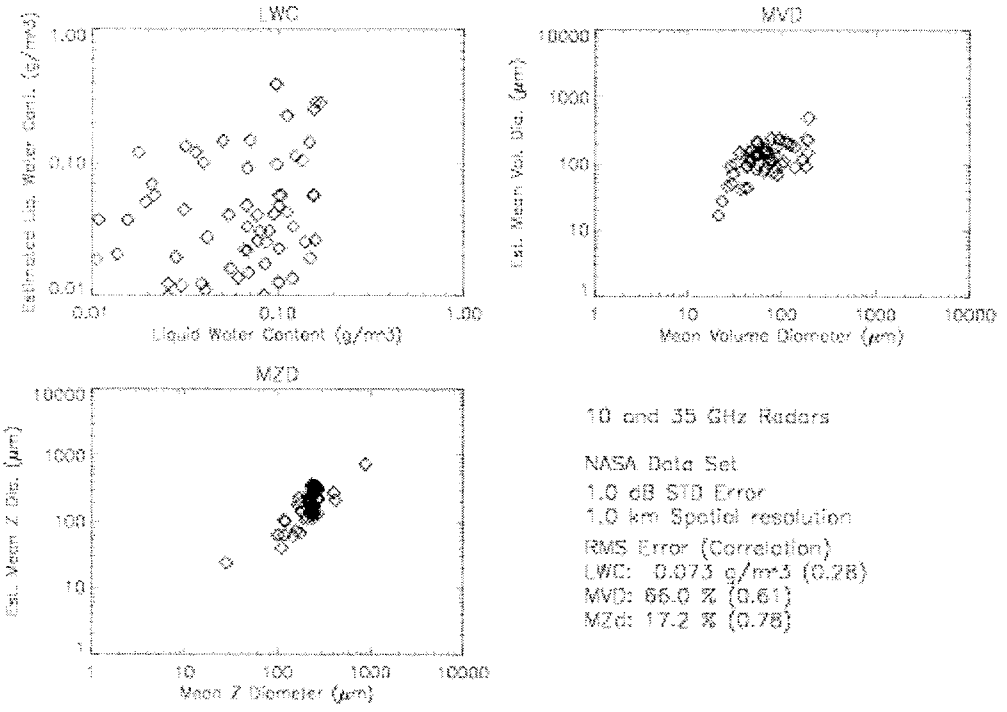

FIGURE A-30. 10-35 GHz RADARS, 500-m RANGE RESOLUTION, 0.5-dB STD MEASUREMENT NOISE, SMALL DROPS AND LOW LWC

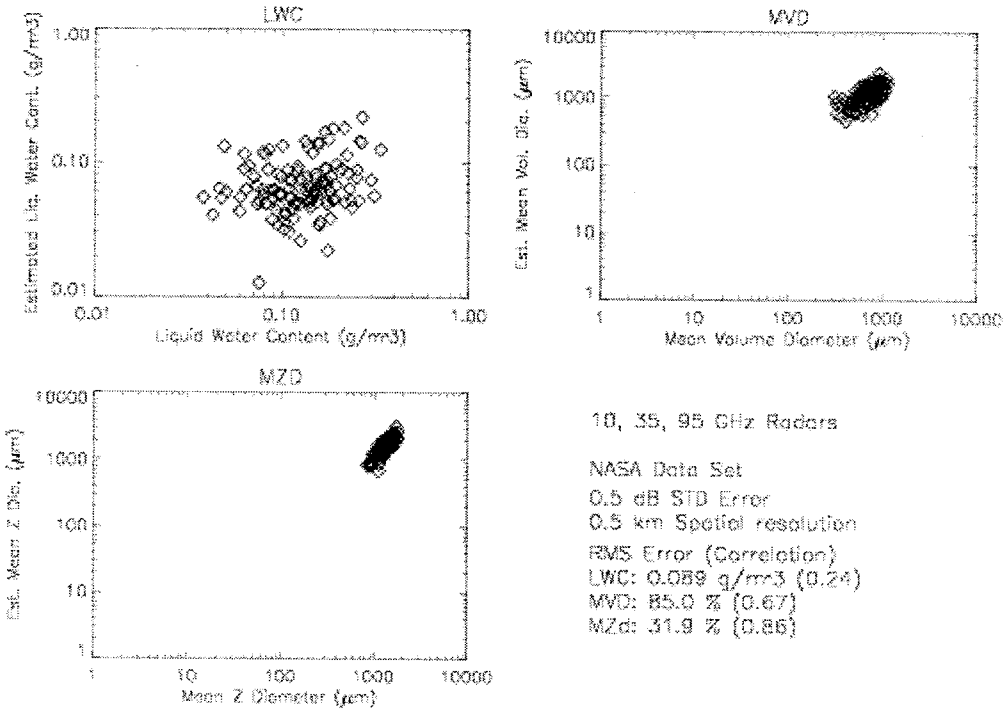

FIGURE A-31. 10-35-95 GHz RADARS, 500-m RANGE RESOLUTION, 0.5-dB STD MEASUREMENT NOISE, LARGE DROPS

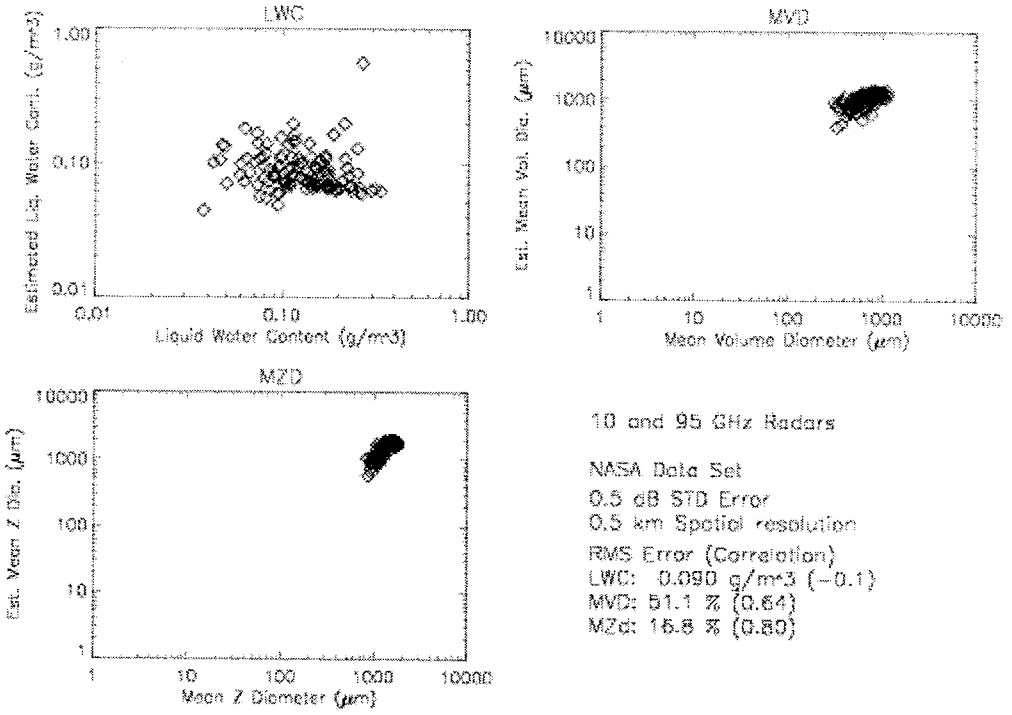

FIGURE A-32. 10-95 GHz RADARS, 500-m RANGE RESOLUTION, 0.5-dB STD MEASUREMENT NOISE, LARGE DROPS

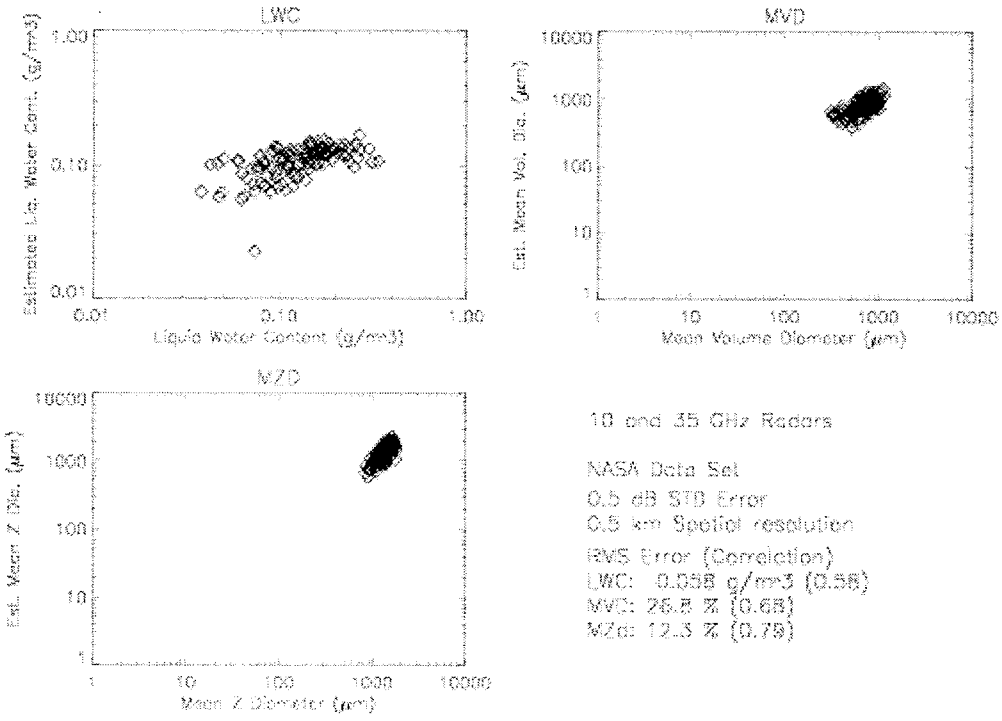

FIGURE A-33. 10-35 GHz RADARS, 500-m RANGE RESOLUTION, 0.5-dB STD MEASUREMENT NOISE, LARGE DROPS

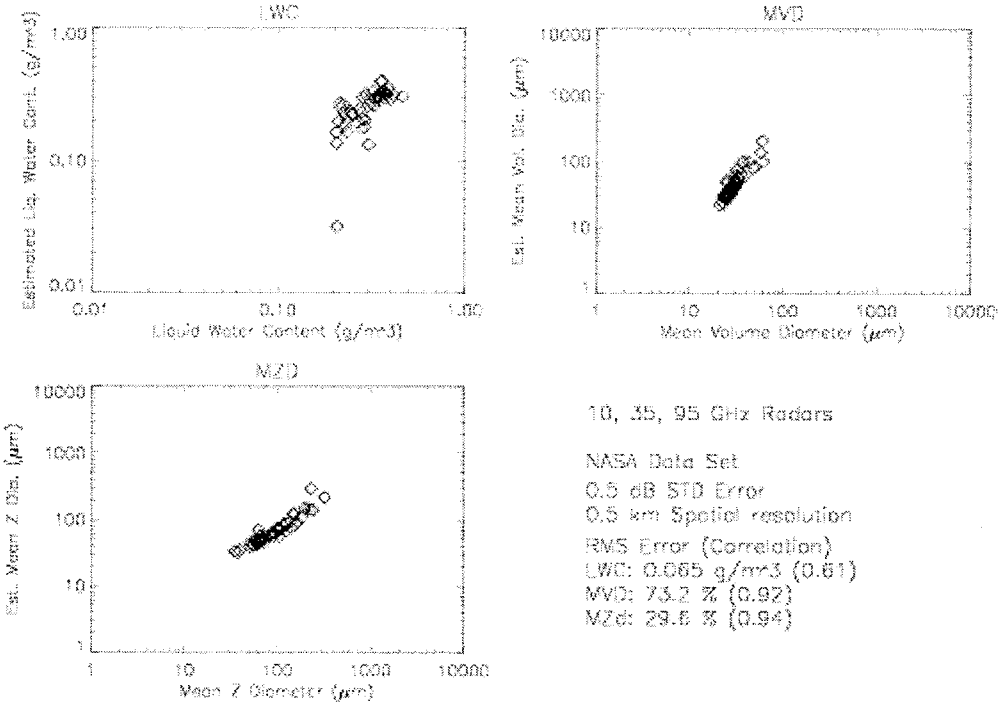

FIGURE A-34. 10-35-95 GHz RADARS, 500-m RANGE RESOLUTION, 0.5-dB STD MEASUREMENT NOISE, SMALL DROPS AND HIGH LWC

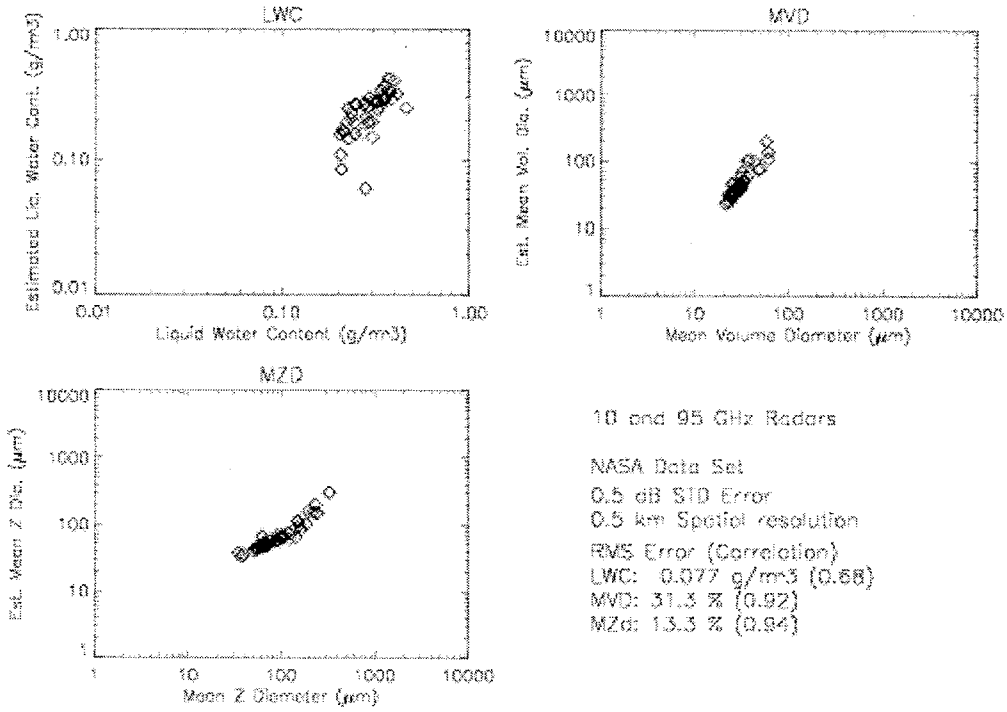

FIGURE A-35. 10-95 GHz RADARS, 500-m RANGE RESOLUTION, 0.5-dB STD MEASUREMENT NOISE, SMALL DROPS AND HIGH LWC

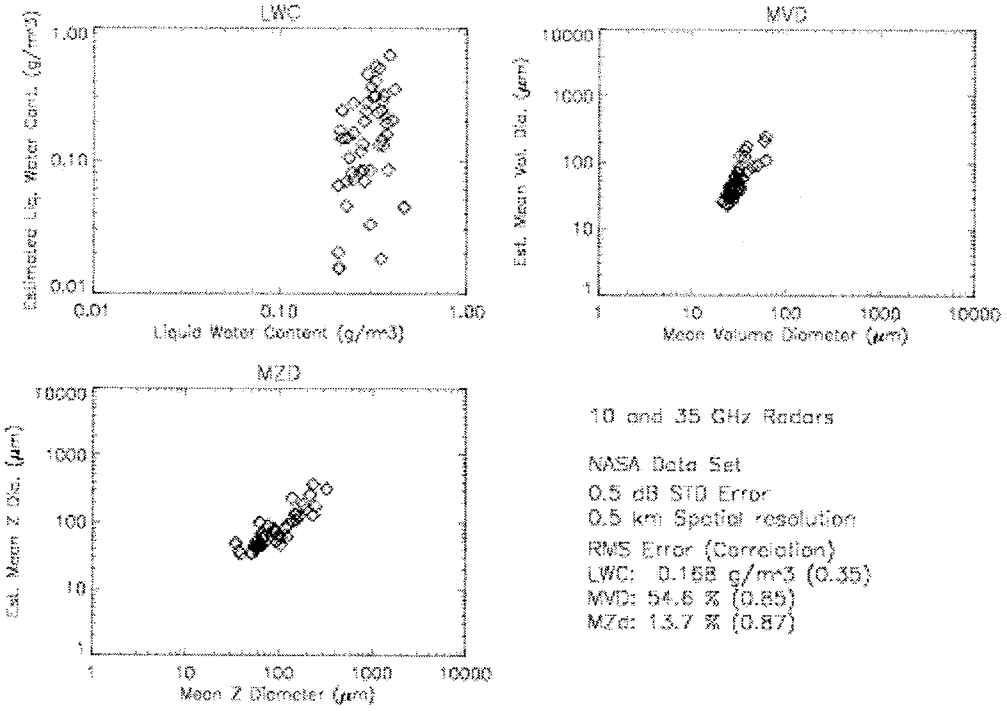

FIGURE A-36. 10-35 GHz RADARS, 500-m RANGE RESOLUTION, 0.5-dB STD MEASUREMENT NOISE, SMALL DROPS AND HIGH LWC